Norwegian University
of Life Sciences

Structure of Native Copper Nitrite Reductase from Alcaligenes faecalis and the Active Site Mutants Asp98Glu and Asp98His

Anine Sætrang

Chemistry and Biotechnology

.

I

.

Acknowledgments

Abstract

Copper-dependent nitrite reductase from *Alcaligenes faecalis* (Cu-*Af*NiR) is an enzyme that catalyzes the reduction of nitrite into nitric oxide. A highly conserved residue, Asp98, in the Type-2 Cu active site, is the proton donor in this reaction. Mutating this residue may cause a shift in the activity of the enzyme, enabling it to reduce other small molecule substrates.

In this thesis, Asp98 has been mutated to Glu and His, respectively, resulting in the Cu-*Af*NiR D98E and Cu-*Af*NiR D98H mutants. The D98E mutant repositions the carboxyl group that acts as an acid/base catalyst in the active site and the D98H both repositions and alters the pK_a of the active site acid/base catalyst. Also, other uncharacterized NiR variants in nature display glutamate and histidine in the Asp98 position. Crystals of the enzymes were soaked in formate to bind formate in the active site. Formate is a possible product in the reduction of CO_2, a small molecule substrate of high interest. The enzymes were also soaked in reducing conditions. The WT and mutants have all been structurally determined by X-ray diffraction. The binding of the transition metals Ni and Co which have different redox properties than Cu was also considered.

Glu98 and His98 both coordinated the Cu atom in the Type- 2 Cu active site in the mutated enzymes. This created new active sites of Cu-*Af*NiR, with possible changes in the function of the enzyme. The oxidized Cu-*Af*NiR WT was the only structure where formate would bind in the active site. The reduction of the enzymes was not fully successful, even with two different methods for reducing the crystals.

Mutating the highly conserved Asp98 in the active site of Cu-*Af*NiR changes the structure, causing the enzyme to not bind formate in the active site as the WT is able to do. This may have implications for the activity of the enzyme. An activity assay of the mutants would determine if they were inhibited from the nitrite reduction, and or are able to catalyze other reactions. A new method of reducing the crystals is also needed, as they were not fully reduced.

.

Abstrakt

Kobber avhengig nitritt reduktase fra *Alcaligenes faecalis* (Cu-*Af*NiR) er et enzym som katalyserer reduksjonen av nitritt til nitrogenoksid. Den svært konserverte aminosyren, Asp98, i Type-2 Cu aktivt sete, er protondonor i denne reaksjonen. Mutering av denne aminosyren kan endre aktiviteten til enzymet, mot å muligens redusere andre små molekyl-substrater.

I denne masteroppgaven ble Asp98 mutert til Glu og His, noe som skaper hhv. mutantene Cu-*Af*NiR D98E og Cu-*Af*NiR D98H. D98E mutanten reposisjonerer karboksylsyregruppen som fungerer som en syre/base katalysator i det aktive setet, og D98H mutanten reposisjonerer og endrer pK_a til syre/base katalysatoren i det aktive setet. Enkelte ikke-karakteriserte NiR- enzym varianter i naturen har også glutamat og histidin i Asp98 posisjonen. Noen av enzym-krystallene ble lagt i format for å binde format i det aktive setet. Format er et mulig produkt i reduksjonen av CO_2, et lite molekyl av høy interesse. Krystallene ble også lagt i løsninger med reduserende forhold. WT og mutantene ble alle strukturelt løst ved hjelp av røntgendiffraksjon. Bindingen av transisjonsmetallene Ni og Co, som har andre redoks verdier enn Cu, i det aktive setet ble også gjort rede for i denne oppgaven.

Glu98 og His98 koordinerte begge Cu atomet i Type- 2 Cu aktivt sete i de muterte enzymene. Dette skapte nye aktive seter i Cu-*Af*NiR, med mulige endringer I funksjonen til enzymet. Oksidert Cu-*Af*NiR WT var den eneste strukturen hvor format ville binde seg i det aktive setet. Reduksjonen av enzymene var ikke vellykket, selv med to ulike metoder for å redusere krystallene.

Mutering av den svært konserverte Asp98 i det aktive setet i Cu-*Af*NiR, endrer strukturen og fører til at enzymet ikke binder format i det aktive setet slik som WT gjør. Dette kan ha betydning for aktiviteten til enzymet. Et aktivitets-assay av mutantene vil kunne påvise om mutantene er inhibert fra å katalysere nitritt reduksjon, og eller om de kan katalysere andre reaksjoner. En ny metode for redusering av krystaller bør også utredes, da metodene i denne oppgaven ikke var vellykkede.

.

Table of Contents

.

Abbreviations

Af-NiR	Nitrite reductase from *Alcaligenes faecalis*
BL21	Type of *E. coli* cells
CO_2	Carbon dioxide
CPD	Cysteine Protease Domain
Cu- *Af*NiR	Copper-dependent nitrite reductase from *Alcaligenes faecalis*
Cu-NiR	Copper dependent nitrite reductase
D98E	Mutation of aspartic acid to glutamic acid in amino acid number 98
D98H	Mutation of aspartic acid to histidine in amino acid number 98
DNA	Deoxyribonucleic acid
E. coli	*Escherichia coli*
F.T.	Fourier transform
FT	Flow Through
g	The gravitational constant, 9.8 m/s^2
H_2	Hydrogen molecules
HDCR	Hydrogen-dependent CO_2 reductase
IPTG	Isopropyl β-D-1-thiogalactopyranoside
LB media	Lysogeny broth
LIC	Ligation-independent cloning
LOHC	Liquid organic hydrogen carrier
nirK	Nitrite reductase K gene
Ox	Oxidized
PCET	Protein coupled electron transfer
PI	Principal investigator
pKa	Acid dissociation constant
Rcf	Relative centrifugal force
Red	Reduced
rpm	Revolutions per minute
SEC	Size-exclusion chromatography

.

SOC	Super Optimal Catabolite
TB media	Terrific Broth
TOF	Turnover frequency
Top 10 cells	Type of *E. coli* cells
WT	Wild type
X-ray	X-ray radiation
Å	Ångstrøm

1 INTRODUCTION

The work in this thesis is a part of the project COOFIX at KBM, NMBU, where Åsmund Røhr Kjendseth is the PI. The project aims to develop a novel enzyme that can reduce carbon dioxide (CO_2) into valuable products such as formate or carbon monoxide. These products can then be used in the chemical industry. The project also aims to make photosynthetic organisms more effective using these enzymes, bypassing rubisco. To achieve this, a range of methods within molecular- and structural biology and biochemical and computational chemistry is applied. Extensive screening methods will then be used to test the enzyme candidates' ability to reduce CO_2. An array of redox enzymes with activity towards small molecules are tested and mutated in the project.

Using CO_2 as a substrate is beneficial as it is an abundant molecule in our atmosphere due to increasing emissions. Converting CO_2 to other chemicals can also be economically beneficial, as the products hold value in several chemical productions. Formate can be useful as a substrate in chemical and biotechnological processes to make valuable products. These products can be used in the food industry, fuel industry, fermentation, and de-icing of the runway at airports (Schwarz et al., 2018). In the fuel industry, there is a shift from using fossil fuels to finding more sustainable alternatives. One of these alternatives is hydrogen molecules (H_2), but there are a few challenges to overcome with using H_2. Using a liquid organic hydrogen carrier (LOHC), like formic acid, the fuel will be easier to store, handle and utilize (Schwarz et al., 2018). Formic acid (HCO_2H) can be deprotonated to formate (HCO_2-), with formate being favored in acidic conditions (Fujita et al., 2013).

This thesis will focus on the copper-dependent nitrite reductase from *Alcaligenes faecalis* (Cu-*Af*NiR or *Af*NiR) (Figure 1.1), encoded by the nitrite reductase gene *nirK*. Both the wild type (WT) and two mutants were purified and crystallized for X-ray crystallography experiments. The amino acid number 98 in solved structures, aspartic acid (Asp, D), is substituted with glutamic acid (Glu, E) and histidine (His, H) respectively in the mutants, and they are therefore named D98E and D98H after their substitution. There is an interest in understanding how the mutation of the amino acids in the active site of the enzyme affects the activity of the enzyme.

They have different pKa values (Table 1.1)and will therefore be different as proton donors. The position of the carboxylic acid group will also differ from Asp to Glu. Other amino acids and the chemical environment in the active site will also affect the pKa values. Their size and structure are also quite different (Figure 1.2)

There is also an interest in investigating the effect of the transition metal within the active site. The NiR used in this project naturally contains copper (Cu), but the effect of transition metals like Nickel (Ni) and Cobalt (Co) in the active site is also briefly considered in this thesis.
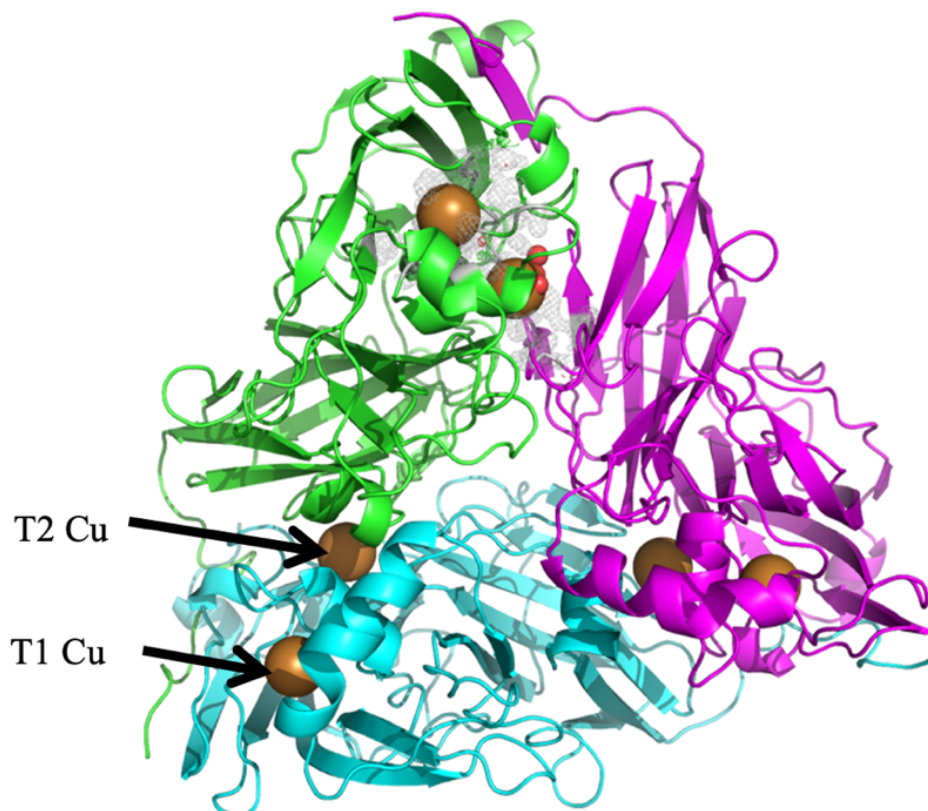
Figure 1.1. *NiR with each of its monomers colored. Cu atoms are enlarged for visibility. The Cu closest to the "corner" of each monomer is the Type-1 Cu site, while the Cu closest to the middle of the enzyme in each monomer is the Type-2 Cu site. In the figures, the active sites Type-1 Cu site and Type-2 Cu site are labeled T1 Cu and T2 Cu respectively.*
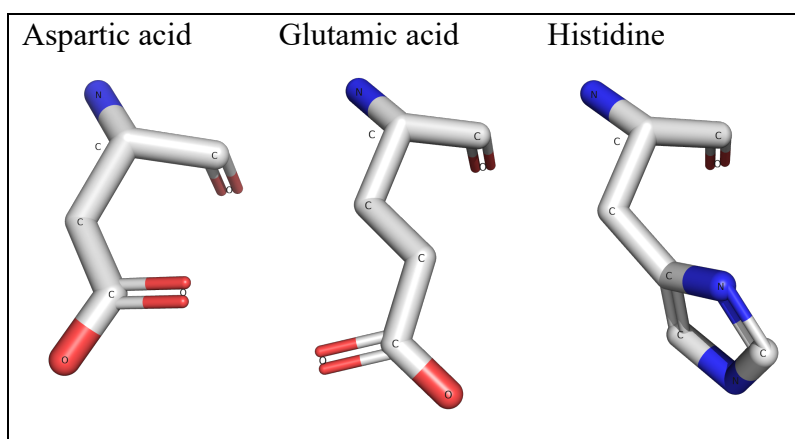
Figure 1.2. The amino acids that are focused on in this thesis. Aspartic acid is the amino acid in the WT of the Af-CuNiR in the structural amino acid number 98. Glutamic acid and histidine are mutated into the amino acid number 98, resulting in what is called Af-CuNiR D98E and Af-CuNiR D98H respectively. The amino acids are structurally different, with Glu and His being a lot bigger than Asp.

Table 1.1. PKa values for the selected amino acids. The change of amino acids with different pKa in the active site can change the pH in the active site.

Amino acid	pK_a side chain group
Aspartic acid	3.65
Glutamic acid	4.25
Histidine	6.00

1.1 Copper dependent Nitrite reductase from Alcaligenes faecalis

Nitrite Reductase (NiR) is an enzyme made of three identical monomers, making it a homotrimer. NiRs that contain multiple copper atoms are called copper-containing nitrite reductase (Cu-NiR), and they are encoded by the gene called *nirK*. (Rose et al., 2021). Each monomer has one electron acceptor site and one active site that each contains a copper ion (Tocheva et al., 2008).
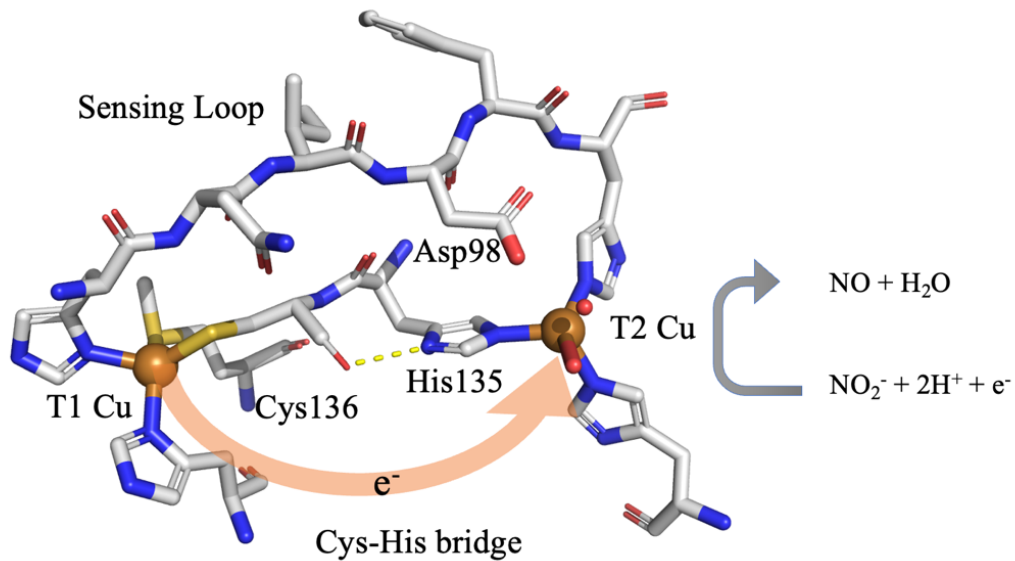
Figure 1.3. *A closer look at the Type-1 Cu site on the left and the Type-2 Cu site on the right. The sensing loop, in which Asp98 is a part of, connects the two copper ions. The electron bridge, Cys-His bridge, also connects the two Cu atoms and transfers electrons from Type-1 Cu to Type-2 Cu where nitrite is reduced to nitric oxide.*

These sites are called Type-1 Cu and Type-2 Cu respectively, and they are connected by a Cysteine-Histidine (Cys-His)- bridge and a sensing loop as seen in Figure 1.3 (Cristaldi et al., 2018). The Type-1 Cu is characterized by a single copper atom coordinated by two histidine residues and a cysteine residue in a trigonal planar geometry with an axial methionine ligand. The Type-2 Cu is coordinated in a distorted tetrahedral geometry by three histidines and a water molecule. Both copper ions are oxidized in the resting state of the enzyme. (Tocheva et al., 2008). The Cys- His bridge is 12 Å and is responsible for transporting electrons from the Type-1 Cu located approximately at the surface of the enzyme to the Type-2 Cu located approximately in between two monomers (Rose et al., 2021). The electrons are needed in the

4

Type-2 Cu site to catalyze the reduction of nitrite (NO_2^-) to nitric oxide (NO) as shown in Figure 1.3.

Some studies have previously suggested that the electron transfer (ET) occurred before the proton transfer (PT) in separate steps in the reaction, but a more recent study using quantum mechanics / molecular mechanics (QM/MM) has shown that while the PT and ET do not happen at the same time, they are dependent upon each other. This is called the proton-coupled electron transfer (PCET) (Cheng et al., 2020). The role of Asp as a proton donor in the reduction of nitrite is shown in Figure 1.4 (Li et al., 2015).
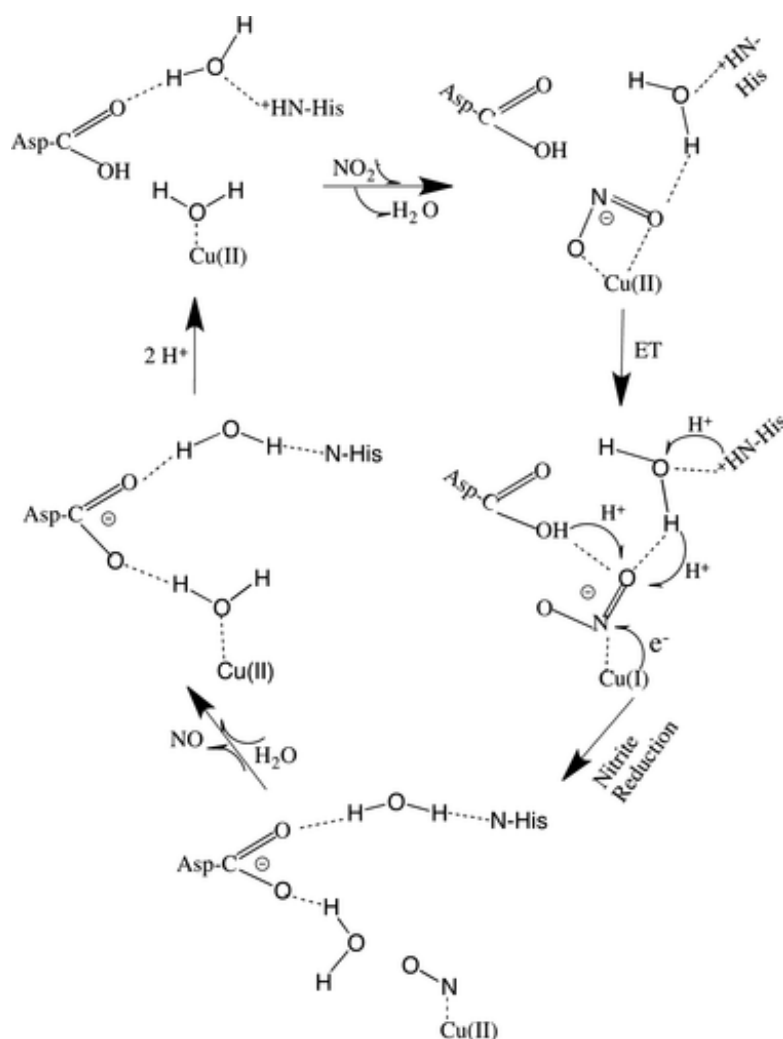
Figure 1.4. *Reaction mechanism of Cu-NiR. Asp98 is the proton donor of the reduction of nitrite to nitric oxide. Reprinted with permission from Biochemistry 2015, 54, 5, 1233–1242. Publication Date: January 16, 2015. https://doi.org/10.1021/bi5007767 Copyright © 2015 American Chemical Society.*

Several residues in the active site have been proven to be critical for the function of the enzyme by providing steric control, substrate binding, and catalytic effect by providing protons to the reaction. (Rose et al., 2021). Several of these residues are highly conserved through evolution, indicating that they are vital for the function of the enzyme. One of these residues in the Type-2 Cu site, isoleucine (Ile) 257, is also conserved, making it a likely important residue for the function of the enzyme. Mutating Ile257 changes the position of the residue and therefore the activity, but the substrate will still bind to the site (Boulanger & Murphy, 2003). Other conserved residues include Aspartic acid (Asp, D) and His, which binds the substrate and donates protons to nitrite. In the Type-2 Cu site of AfNiR, these are called Asp98 and His255 (Kataoka et al., 2000). Mutating these have shown that they are vital to the activity, as the activity decreases as a result of their substitution to other residues, and the structure in the active site is also reoriented (Boulanger et al., 2000). In the PCET, the Asp98 is the proton source, but the PT only happens after the ET. The first step is nitrite binding, which causes the distance between the Asp98 and the O_2 to decrease until its 1.70 Å. This causes an elevation of the reduction potential of the Type-2-Cu active site and the long-range ET from Type-1 Cu to Type-2 Cu can happen. After the ET, the PT from Asp98 to nitrite occurs (Cheng et al., 2020). Given how central these residues are for the activity of the protein, that is where they have been mutated to change the enzyme´s activity from reducing nitrite to reducing CO_2.

1.2 Directing the activity of copper dependent nitrite reductase toward CO_2.

The ligand Asp98 in the Type-2 Cu site is vital in reducing nitrite in Cu-NiR, and mutating it changes the activity of the enzyme (Boulanger et al., 2000). By mutating it to a Glu and His, making the mutants D98E and D98H respectively, the hope is to change the enzyme's ability to reduce nitrate and rather reduce CO_2. These variations of Cu-NiR where Asp98 has been naturally evolved to Glu and His have also been found in sequence data. This is indicating that the enzyme might function even with these variations in essential positions. These variations have been found using tools developed by Åsmund Røhr Kjendseth. Putative NiR-sequences were analyzed to see what variations occur. Only one D98E, but several D98H were found. It is not known what activity these naturally mutated enzymes have.

1 INTRODUCTION

Cu-NiR was chosen as a candidate for several reasons. Both nitrite and the carbon dioxide radical anion are small molecules with similar shapes. Cu-NiR is already able to reduce nitrite, and the carboxyl radical is an intermediate in the reduction of CO_2. A similar shape may make it easier for Cu-NiR to change its substrate and product, without changing the entirety of its active site and structure. The reaction is also similar because the Cu-NiR naturally reduces nitrite to nitric oxide using one electron, and the reaction also includes PT. The reduction of CO_2 to formate requires a formal hydride transfer, i.e., two electrons and one proton (Costentin et al., 2013; Yang et al., 2020). Cu-NiR is also able to bind formate in its active site (Tocheva et al., 2008). Formate is a possible product in the reduction of CO_2 and can be a substrate in other value-added processes (Schwarz et al., 2018). CO_2 is an inert and stable molecule as a result of the energy required to bend the molecule to the radical that is needed for the reduction to formate (Leung & Ho, 2019). Table 1 in (Windle & Perutz, 2012) shows the reduction potential for the following reactions Eq. 1-3.

$$CO_2 + e^- \rightarrow CO_2^{\bullet-} \qquad\qquad E° = \text{-1.9 V} \qquad\qquad \text{Eq. (1)}$$

$$CO_2 + 2H^+ + 2e^- \rightarrow HCO_2H \qquad\qquad E° = \text{-0.61 V} \qquad\qquad \text{Eq. (2)}$$

$$CO_2 + 2H^+ + 2e^- \rightarrow CO + H_2O \qquad\qquad E° = \text{-0.53 V} \qquad\qquad \text{Eq. (3)}$$

A trend in the reduction reactions of CO_2 is that the reduction potential is higher in the reactions that require more protons and electrons. These reactions require an overpotential, and therefore a lot of energy (Leung & Ho, 2019). Solutions for the hydrogenation of CO_2 exist. Among them are multiple chemical catalysts, but they often require conditions that are expensive and energy-consuming. A biocatalyst called hydrogen-dependent CO_2 reductase (HDCR) has been described as better than chemical catalysts when it comes to turnover frequency (TOF) and conditions for the reaction. They are sensitive to oxygen, so large scale CO_2 reduction is difficult (Leo et al., 2021). To compete with fossil fuel, sustainable alternatives need to be cost-effective and use less energy in the production (Schwarz et al., 2018).

The reduction potential of the reactions is used to determine a catalyst's efficiency. In nature, several enzymes are used to catalyze reactions over a range in reduction potential, as they are

somewhat specific to a certain potential. By mutating 5 residues and using the metal ions Cu and Ni, the protein azurin nearly covers 2V of the range in the reduction potential (Hosseinzadeh et al., 2016). This illustrates the viability of tuning the redox potential of a metalloenzyme by mutating a few active site residues and changing the transition metals in the enzyme. Such a change in potential may also alter the activity of the enzyme towards other substrates. By swapping Cu with other transition metals such as Ni in AfNiR it can drastically change NiR's ability to reduce nitrite. The aim is to find mutation and transition metal combinations that alters the activity of *Af*NiR in favor of CO_2 reduction.

1.3 Method-related theory

1.3.1 X-ray crystallography

crystallography can together with recombinant DNA technology provide structures of biological molecules at atomic resolution. It is therefore the preferred way of studying the structure of proteins, as other methods will not provide the same precision (McPherson & Gavira, 2014). Furthermore, X-ray crystallography is used to investigate interactions between molecules such as an enzyme´s substrate binding and catalytic ability (McPherson, 1989).

Although X-ray crystallography provides an image of the structure of macromolecules, it is not an image in the literal sense like magnified images provided by microscopes. Molecules are simply too small to be visible with a microscope using visible light as the atoms are bonded together as small as 1-2 Å (1 Å = 0.1 nm) apart while visible light has a wavelength of 350 – 700 nm. X-rays are therefore used instead because they have wavelengths that range the most suitable for atom size, 0.5 -1.6 Å. A microscope uses lenses to focus the light and create a magnified image of the object, but making lenses that focus the diffracted X-rays has proven difficult. The diffracted X-rays are therefore hitting a detector instead, creating a diffraction pattern. The pattern and intensities in the pattern, form the raw data. Through data processing the data will provide an image of the protein structure (Blow, 2002).

The X-rays must be used on crystals of protein, as the radiation damage on one single molecule would be too much to gather data. In a crystal, the number of molecules can be 10^{15} and more, all in order in identical unit cells. Some of the molecules can then be damaged by the radiation without destroying the crystal completely (Blow, 2002). The electrons in the protein will scatter

the X-rays to create a diffraction pattern in a unique shape. The protein must be ordered in a crystal shape with flat surfaces and symmetry where the atoms are arranged in specific space groups for the X-rays to form a distinctive pattern. This diffraction pattern is then used to produce an atomic model of the protein. The diffraction patterns' intensities and angles create an electron density map, which together with the protein sequence and a model of a similar protein structure forms a temporary model, which is then refined in small steps to procure a final model of the protein structure.

Crystallization.

Protein crystallization is viewed as a young and empirical field, meaning it is more based on observations and experiments rather than logic (McPherson & Gavira, 2014). Crystallization can be unpredictable given the unique characteristics of each macromolecule. The exact same conditions used on the same molecule can very well result in different polymorphic forms due to the molecules' different conformations (McPherson, 1989). However, there are a few techniques and methods to help the approach of crystallizing a protein. A good-quality crystal is vital for good-quality diffraction data (McPherson & Gavira, 2014).

A large number of parameters affect the crystallization of proteins, such as temperature, pH, buffers, precipitants, and additives. More importantly, the protein itself must be purified and concentrated. Varying these conditions will help in the search for the correct conditions for crystallizing a specific protein. Optimizing conditions is largely based on trial and error, by systematically screening for conditions that promote crystal growth and improving these conditions until they are optimal for growing good-quality crystals for the specific protein. Another approach to finding the optimal conditions is a shotgun approach using theory or experience to guess the right conditions. This may save time and resources. The screening process is often done by using commercial screening- kits that vary the solution in each well (McPherson & Gavira, 2014).

In vapor diffusion crystallography, a drop of protein solution is placed either on a pedestal by a reservoir making it a sitting drop, or the drop is placed on a cover slide turned upside-down above the reservoir making it a hanging drop. The reservoir will contain the solution of buffer, precipitants, and other additives. The same solution will be mixed with the drop of protein, making the concentration of the reservoir solution in the drop a lower concentration than the

same solution in the reservoir. The concentration of protein in the drop is also decreased. Water from the drop will evaporate due to the difference in concentration between the drop and the reservoir. An equilibrium between the reservoir and the drop of protein is established. The concentration of both the precipitant and protein in the drop will increase.

The change in concentration of the protein and precipitant will change the solubility of the solution, causing the solution to become supersaturated which is vital for crystallization. The supersaturation of the protein solution will make the molecules pack in repeating patterns, creating crystals. The shape, size, and color of the crystals vary depending on different proteins. The conditions in which the crystals are supersaturated is the driving force behind the two steps of crystallization: nucleation and crystal growth. Nucleation happens as the concentration of protein and precipitant increases. Critical nuclei are formed orderly as the protein assembles.
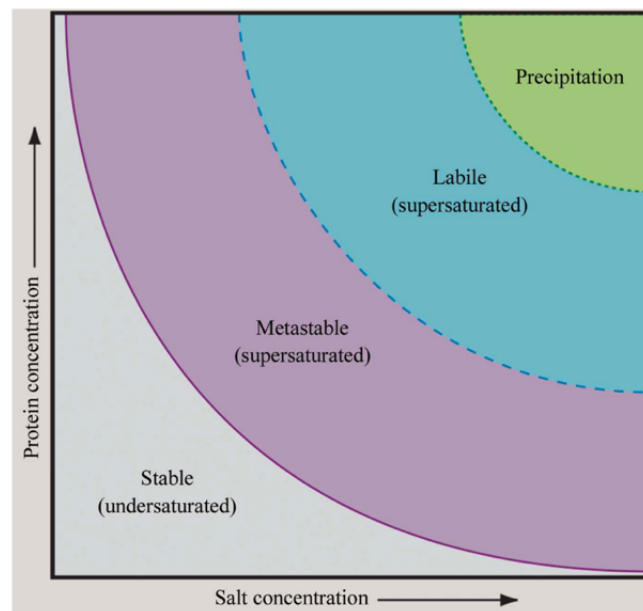
Figure 1.5. The figure shows how the solubility of the protein solution is affected by the concentration of protein and salt. This provides a visual representation of how supersaturation of the protein will promote crystal growth, by moving between the phases due to the changes in concentrations. The image is reproduced with permission of the International Union of Crystallography (McPherson & Gavira, 2014).

The aggregation of the protein causes the concentration of protein in the solution to decrease, and the system is now in the metastable zone (Figure 1.5) and growth phase of the crystals (McPherson & Gavira, 2014).

X-ray diffraction, data collection, and data processing.

Electromagnetic waves are photons, both particles and waves, and the X-ray photons that come across electrons in a molecule will be absorbed by the electrons, who will then vibrate and emit the same energy and wavelength in the form of an X-ray photon, but in a new direction, causing what is called coherent scattering. This coherent scattering is used to determine the structure. There is also incoherent scattering, caused by photons of lower energy being emitted by the electrons that are in atomic orbitals, resulting in radiation damage on the crystal. The X-rays also encounter the nucleus, in addition to the electrons, but the photon scatter is insignificant as the large size of the nucleus causes it to vibrate much less when hit by the X-ray photon (Blow, 2002). The coherent scattering is detected as diffraction patterns like spots of diffraction maxima. The detector measures the intensities of the maxima. During this data collection, the crystal is rotated (Powell, 2017). The rotation causes the X-ray beam to hit the crystal in many directions, causing collected patterns from a wide range of directions, making the resulting structure a three-dimensional structure (Blow, 2002).

The data collected from the X-ray diffraction must be processed by computer programs because of the large volume of the raw data (Blow, 2002). There are several software packages to choose from. The diffraction images are processed by first finding the spots and indexing them, resulting in an estimate of the dimensions of the unit cell and the orientation of the crystal. The next step of the processing is parameter refinement, followed by integration where the intensities of the diffraction spots are measured. The data must also be scaled correctly, resulting in statistics like R values and correlation coefficients which are important for validating the quality of the data. Lastly, the merging of reflections of measurements of the same symmetry is done. This data processing is now an automated process at the synchrotrons, with pipelines processing the data at a high speed while the user is collecting data at the beamline. Several pipelines are available, and the user must choose which datasets to work with based on their statistical results. In this thesis, the highest resolution with the best completeness was chosen (Powell, 2017).

Phasing and molecular replacement

Electromagnetic waves like X-rays are described by their phase and amplitudes, of which the amplitude is translated into the intensity of the diffraction pattern spots. The square root of the intensity is proportional to the amplitude, and the intensity is a measurement of how many electrons there are present at a specific point in the crystal. The phases of the electromagnetic waves, however, are lost, creating what is called the phase problem (Taylor, 2010). The phase problem in X-ray crystallography stems from the inability to observe the phases of X-rays. To overcome this problem, the phase must be found indirectly (Blow, 2002). In this thesis, the phases were found using molecular replacement. Since the structure of the WT of the protein is known, the atomic coordinates of this structure were used as a similar structure to find the phases (Taylor, 2010). Knowledge of a similar structure can be used together with the amplitude, to find the phases. The phases will then together with the amplitude provide the electron density, through the Fourier transform (F.T.)

Refinement and model building.

After choosing a dataset with high resolution and completeness and performing molecular replacement using a similar protein structure, the density map and approximate structure of the protein are obtained. This structure will need refinement in small steps to make sure the changes made are beneficial to the model building. The R_{free} value and R_{work} value give insight into the relationship between the experimentally recorded density map and the approximated model structure. How well the model fits into the density map, shows the accuracy of the model. This is measured by the R – values (Brünger, 1992). By making small changes to the structure by adding or removing amino acids, changing the angles and rotamers of some amino acids, adding missing molecules to better fit the density, and refining in between the changes, the R-values are hopefully lowered to a satisfactory value (Wlodawer et al., 2013). In this thesis, the maximum R_{free} value was calculated using the resolution of the chosen dataset, divided by 10, and 0.05 added.

2   AIMS OF STUDY

This thesis aims to structurally characterize two mutants of copper-dependent nitrite reductase from Alcaligenes faecalis (*Af*NiR). Both reduced and oxidized crystals, as well as crystals with and without formate of the WT Cu-*Af*NiR, D98E Cu-*Af*NiR, and D98H Cu-*Af*NiR, will be structurally determined to research the effect of mutating conserved active site residues. Additionally, crystals where cobalt or nickel are added to the as-purified enzyme to evaluate the ability of *Af*NiR to bind these transition metals.

Expression and purification of mutants of *Af*NiR.

Asp98, amino acid number 98 in solved structures of *Af*NiR, is a highly conserved residue in the Type-2 Cu active site and responsible for hydrogen donation in the reduction of nitrite. The project aims to mutate this amino acid to Glu (D98E) His (D98H), as well as express and purify the enzymes for use in crystallographic studies to research how these mutations affect the structure of the active site of the enzyme.

Transition metal in the active site.

The *Af*NiR made from the *nirK* gene normally has Cu in the active site, and most crystals are made with Cu-saturated protein. However, there is an interest in researching how a different transition metal in the active site would affect the structure and activity of the enzyme. *Af*NiRs ability to bind Co in Ni in the active site is therefore considered briefly.

Treatment of crystals before cryofreezing.

The Cu-*Af*NiR crystals will be soaked in various solutions to create conditions for the enzyme to be reduced, oxidized, and bind to formate. The solved structures will then be compared to each other to show how the soaking affected the enzyme, as well as compared to existing structures to research if the desired effect of the soaking was obtained.

3 MATERIALS AND METHODS

All buffers and solvents used are in the appendix.

3.1 Preparation of protein

3.1.1 Plasmid transformation

The plasmid transformation into TOP10 cells *Escherichia coli* (*E. coli)* was done by Eirin Landsem. The WT sequence of the *nirK* gene was ordered from Invitrogen and NEBuilder was used to incorporate the gene into the plasmid pET22b-CPDBamHI-Leu. This plasmid contains a Cysteine Protease Domain tag (CPD-tag) which is a C-terminal 6xHis-tagged inducible auto-processing enzyme tag that improves the solubility and protein yield in recombinant protein expression and purification. The His-tag can cause problems when it comes to crystallization, so it needs to be removed during the purification (Biancucci et al., 2017). The ligated plasmid was then transformed into chemically competent TOP10 cells, which are used for high-efficiency cloning and plasmid propagation. Ten colonies were picked for colony PCR. Colonies showing the right-sized insert were used to inoculate 4 mL LB media and grow overnight. Plasmids were thereafter extracted and sequenced before transformation into chemically competent BL21 cells, which are used to overexpress the proteins.

Transformation in BL21 cells.

Purified plasmid (10 ng) was mixed gently with 25 µL chemically competent E. coli BL21 DE3 cells in a microcentrifuge tube and kept on ice for 30 minutes. The tube was then placed in a 42°C-water bath for 30 seconds to heat shock the cells. The transformation reaction was placed on ice for 2 minutes, followed by the addition of 250 µL S.O.C at 37°C and placed in a thermomixer for one hour (37 ℃, and 750 rpm).

Agar plates with 100 µg/mL ampicillin for the pET22b vector were heated to room temperature before 100 µL and 150 µL of transformed E. coli were spread out on the plates. This was done with a sterile technique using ethanol and a Bunsen burner. The plates were allowed to dry before they were incubated at 37 ℃ overnight. The plates grew colonies, confirming they were transformed.

3.1.2 Protein expression

Small-scale growing with expression test was performed before growing large scale. LB media (2 mL) with 100 μg/mL Amp was added to autoclaved culture tubes and a toothpick was used to inoculate a colony in the media. Five colonies from each mutation were chosen for the small-scale growing. The tubes were incubated at 200 rpm and 37 °C overnight. The O/N culture (1 mL) was added to tubes with 0.7 mL 50 % autoclaved glycerol and frozen at – 80 °C to make glycerol stocks.

The overnight culture (50 μL) was added to autoclaved culture tubes with 1 mL LB and 100 μg/mL ampicillin and the tubes were incubated for 2 hours at 37 °C, 200 rpm. One culture from each mutant had a replica that was not induced as a control. One of the two tubes was then induced with 0.25 mM IPTG using 0.5 μL from 0.5M stock, while the other tubes were not induced. They were then incubated at 20 °C overnight. The culture was then moved to 1.5 mL Eppendorf tubes and spun for 30 seconds, and the supernatant was decanted. The induced samples were then resuspended in 0.5 mL binding buffer and sonicated on ice for 20 seconds, 20 % amplitude, 2 seconds on and 2 seconds off. They were then spun for 3 minutes at maximum speed and the supernatant and pellet were separated into a soluble fraction (supernatant) and an insoluble fraction (pellet), called S and NS respectively. NS fraction was resuspended with Milli-Q to a total volume of 1 mL, spun for 3 minutes at max speed and the supernatant was decanted. Two Mini-PROTEAN TGX Stain-Free gels with 15 wells were used in an SDS-Page.

Gel 1 was made using cultures with mutant D98E, and gel 2 was made using cultures from mutant D98H. Numbers 1-5 in each gel are the different colonies from the transformation. The samples on the SDS-Page were prepared by adding 100 μL Milli-Q to the pellets and resuspending them. Part of the resuspended pellets (4 μL) were then added to PCR tubes and mixed with 3 μL SDS sample buffer and 5 μL Milli-Q. SDS sample buffer (3 μL) and 9 μL of soluble fraction sample were added to PCR tubes. The tubes were then incubated at 95 °C for 10 minutes. The samples (10 μL) were then loaded onto the gel along with 5 μL of the ladder. The gel was then run for 30-40 minutes at 200 V. The SDS- Page from the expression test is in appendix.

Growing large scale:

Overnight culture:

When growing the enzymes, both the wild type and the mutants, 50 mL of LB media and 50μL from 100 mg/mL ampicillin were added to Erlenmeyer flasks, creating a concentration of 100 μg/mL ampicillin. An autoclaved toothpick was swirled in the chosen glycerol stock and added to the flask. This was then incubated at 200 rpm and 37 °C overnight. Glycerol stock used; D98E Colony 2 and D98H Colony 3.

Harbinger bubble system:

TB media (0.5 L) with phosphate buffer was used for growing in a Harbinger bubble system. To the Duran flasks, 500 μL of 100 mg/mL ampicillin, 200 μL antifoam stock, and 25 mL of the overnight culture was added, making the concentration 100 μg/mL ampicillin and 0.01 % antifoam, and 0.03 % ethanol. The flasks were heated in a water bath at 30 °C and the air was added continuously. When the OD was measured at 0.6-0.8 the temperature was lowered to 20 °C and IPTG was added to start the expression. The flasks then stayed in the bubble system overnight.

Harvesting the cells:

The culture was added to 1 L centrifuge tubes and balanced with binding buffer (20 mM MOPS, 20 mM imidazole, 500 mM NaCl, pH 7.4). The centrifuge was pre-cooled, and the tubes were centrifugated for 30 minutes at 4 °C, 5500 g. The supernatant was removed, and the pellet was resuspended with binding buffer to 80 mL. This was divided into two and added to 50 mL falcon tubes. The tubes were then frozen at -20 °C until purification.

3.1.3 Protein purification

Cell lysis & CPD- His purification:

The frozen suspended pellets were thawed before disruption by sonication on ice for 10 min (10 s ON / 10 s OFF cycle, 30 % amplitude) using a sonicator (VCX-500, Vibra-Cell Sonics, USA). Clarified lysate was obtained by centrifugation (30 min, 4 °C, and 20 000 rpm) and added to new 50 mL falcon tubes. A binding buffer was added to a total volume of 50 mL. The lysate was purified by affinity-chromatography, utilizing 5 mL HisTrap™ prepacked nickel columns (Cytiva, Sweden) with a purification robot with a premade fully automatic protocol.

The column was first calibrated with 5 CV of binding buffer before sample application. Unbound protein was washed off the column with 5 CV binding buffer, before 2L cleavage buffer (20 mM MOPS, 20 mM imidazole, 500 mM NaCl, 1 mM phytic acid, pH 7.4) was applied (0.2 mL/min). The phytic acid activates the CPD, which cleaves at an added leucine in a linker region between the protein of interest and the CPD-tag. This results in the protein of interest eluting, while the CPD-6xHis-tag remains on the column. Thereafter, the CPD-tag remaining on the column was eluted into a separate tube with high-imidazole elution buffer (20 mM MOPS, 500 mM imidazole, 500 mM NaCl, pH 7.4) (Biancucci et al., 2017).

The protein was then up concentrated using SEC buffer and Amicon filters 30,000 MWCO. They were centrifuged for 10-15 minutes with 4700 rcf. This was done approximately 3 times, adding more buffer each time. Protein was stored in Eppendorf tubes at 4 °C.

Size-exclusion chromatography (SEC)
This purification separates based on the sizes of the sample- components, as small proteins will enter the porous agarose-dextran composite beads that the column is packed with while bigger components of the sample will travel around the beads. The beads will slow down the protein, making the retention time longer for the protein than the other components.
For the SEC purification, the protein had to be in the SEC buffer (20mM MOPS, 200 mM NaCl, pH 7.5). This was done the same way as the up concentration above. The SEC purification was done on the Äkta go from Cytiva, using the column HiLoad 16/600 Superdex 75 pg. Size: 120 mL and the software Unicorn 7.6. The Äkta protocols were followed, using SEC buffer, and injecting 1 mL of protein. Fractions were collected using the Fraction collector F9-R.

After the SEC, some of the fractions were analyzed using SDS-Page. This was done as a precaution, as there had previously been some issues involving the Äkta system. The SDS-Page was done using the same conditions as the SDS-Page for the expression test. Fractions 2-8 of D98H and a sample of D98E were added to the wells in a gel. Five μL of the ladder was used on the gel. The samples were prepared by adding 3 μL loading dye, 5 μL Milli-Q, and 3 μL fraction to PCR tubes and incubating them at 95 °C for 10 min. The SDS-Page is in appendix.

17

After purification, some of the protein was saturated with 5x Cu and up-concentrated using amicon filters and Tris HCl 7 pH buffer, while another part was up-concentrated the same way without adding Cu. This was later used to saturate with 2.5x Ni. For the saturation, the concentration of the protein was measured using Protein A280 on Nanodrop, with the input 37.03 kDa and 41.37 e/1000, and the Tris-HCl as blank. The concentration of protein was then converted to molar. Five times the M of the protein of Cu was added to the protein, and 2.5 times the M of the protein of Ni was added to the other fraction of the protein. Because the enzyme has 2 Cu sites, the Cu is 2.5 in excess and the Ni is 1.25 in excess.

During the up concentration, the tubes containing Amicon filters 30,000 MWCO were centrifuged for 10-15 minutes with 4700 rcf. This was done 3 times, adding more buffer each time. Protein was stored in Eppendorf tubes at 4 °C.

Crystallization was tested with protein solutions purified with affinity-chromatography and SEC as well as protein solutions only purified with affinity-chromatography. Crystals were obtained in both cases, but the former yielded the largest and best-looking crystals.

3.2 X-ray crystallography

3.2.1 Preparation of protein crystals

Sitting drop.

Commercial screens for finding optimal crystallization conditions were used with sitting drop vapor diffusion crystallization. The screen with the conditions that yielded crystal growth in the WT Cu-NiR, and therefore became the starting point for optimizing the crystallization conditions, was JCSG-plus™ (Molecular Dimentions). Well B6 containing 0.1 M phosphate/citrate buffer pH 4.2 and 40 % v/v ethanol. For WT NiR saturated with Ni, several screens gave some crystal growth. The chosen screen to start optimization from was Index™ HT (Hampton Research). Well F7 containing 0.2 M ammonium sulfate, 0.1 M BIS-TRIS pH 6.5, 25% w/v polyethylene glycol 3.350.

Hanging drop.

Following a screening of the WT Cu-NiR, it was found that 0.1 M phosphate citrate buffer at pH 4.2, 40 % v/v ethanol, and 40 % v/v Milli-Q water as a reservoir solution were a good condition. These conditions were also used for both D98H and D98E. There was also a range of concentrations of reservoir solution with phosphate citrate buffer varying from 0.05-0.16 M

and ethanol varying from 30 – 52 % v/v. Both the fixed concentrations and the variations of concentrations were used on both the WT and the mutants, with varying results.

Hanging drop plates were set up with varying concentrations of drops using 1 µL of 10, 15, 20, and 25 mg/mL protein and 1 µL reservoir solution in the droplets. The different concentrations of protein were prepared from the purified stock solution of protein in Tris- HCl buffer. The dilution of this protein was done with both Milli-Q and buffer, both creating crystals. The cover glass used for hanging drop was Siliconized Glass Circle Cover Slides. (18 mm, Hampton Research). Due to the variation of preparation of the crystals, a variety of crystals were frozen to find their structure using X-ray crystallography.

3.2.2 Crystal freezing

The crystals were soaked in solutions to prepare for freezing. All crystals were soaked in cryo-solution as the last step before being frozen in liquid nitrogen and added to the transportation pucks. The crystals were frozen with loops of different sizes depending on the size of the crystals themselves. The pucks were placed in a tank containing liquid nitrogen until transportation. Before the cryo solution, the crystals were soaked in different solutions to create a variety of conditions for the protein. These include reducing conditions and oxidizing conditions. The solutions were also made with and without formate to create conditions where proteins would bind to formate. The four different soaking conditions for the Cu-containing crystals attempted to create the following proteins: Oxidized protein containing no formate, oxidized protein containing formate, reduced protein containing no formate, and reduced protein containing formate. These conditions were obtained by soaking the crystals in cryo solution, solution 1, solution 2, and solution 3 respectively. The cryo solution contained 30- 32 mg glucose in a 100 µL reservoir solution, creating 0.3 – 0.32 mg/µL glucose solutions. This was sonicated to help dissolve the glucose. Solution 1 contained reservoir solution and 20 mM formate. Solution 2 contains a reservoir solution purged with N_2 and 2 mg sodium dithionite (DT). Solution 3 contained reservoir solution and 20 mM formate purged with N_2 and 2 mg DT. Solutions 2 and 3 were made in two different ways to explore different reducing alternatives and compare them. The crystals in pucks 002 and 003 were soaked in solutions 2A and 3A while the crystals in puck number 006 were soaked in solutions 2B and 3B. Solution 2A and 3A was made partly in the anaerobic work chamber. The reservoir solutions were purged with N_2 outside the anaerobic chamber, using vials with a silicon septum on 1 mL

reaction vials to block oxygen from entering the solution. The DT was added to the solution in the anaerobic chamber, creating 2mg/mL concentration. Solution 3A also contained 20 mM formate. Solutions 2B and 3B were made in a similar way, but the reservoir solution purged with N_2 together with 2 mg DT and 6.8 mg formate was in the anaerobic work chamber overnight before it was mixed, and placed in vials with a septum. The concentration of DT in 2B and 3B was 0.4 mg/mL, and the concentration of formate in 3B was 1.36 mg/mL. Syringes were used to transport the solution from the vials onto the cover slides where the crystals could be soaked in the solutions. All crystals were soaked in cryo solution right before freezing to protect the crystals from liquid nitrogen. The crystals soaked in solutions 2A and 3A were soaked for 5 minutes and crystals soaked in solutions 2B and 3B were soaked for 1-2 minutes. During this time, the cover slides were put onto the well to stop the droplets from drying out. In solutions 2B and 3B, Methyl viologen was added to the vials after the crystals were all frozen. The solution turned blue, indicating that the solution still contained reduced dithionite. The following Table 3.1 shows an overview over the crystals and their soaking treatment.

Table 3.1. Overview of the crystals divided by WT and mutation. The puck they were stored in after freezing correlates to their soaking solution. Reduced crystals placed in pucks 002 and 003 were soaked in solutions 2A and 3A, while reduced crystals in puck 006 were soaked in solutions 2B and 3B. The crystals in pucks 002 and 003 were structurally solved by Anine Sætrang, while the crystals in puck 006 were structurally solved by Eirin Landsem.

Cu-NiR variant	Redox condition	Added formate	Puck	Position in puck	Soaking solution
WT	ox	No	002	1	cryo solution
WT	ox	Formate	002	3	1
WT	red	No	002	5	2A
WT	red	No	006	5	2B
WT	red	Formate	006	6	3B
D98E	ox	No	002	10	cryo solution
D98E	ox	Formate	002	12	1
D98E	red	No	006	7	2B
D98E	red	Formate	006	8	3B
D98H	ox	No	003	1	cryo solution
D98H	ox	Formate	003	4	1
D98H	red	No	006	9	2B
D98H	red	Formate	003	7	3A

3.2.3 X-ray diffraction, data collection, and processing

Beamline ID30B at the European Synchrotron Radiation Facility (ESRF) in Grenoble, France, was used to perform the X-ray crystallography on the protein crystals (McCarthy et al., 2018; Mueller-Dieckmann et al., 2015). The collected data were automatically processed by several softwares in the ESRF user portal. The datasets with the highest resolution, and highest completeness for each crystal, were downloaded.

3.2.4 Structure Determination, refinement, and model building

The Phenix software system (Afonine et al., 2012; Liebschner et al., 2019; Williams et al., 2018) together with Coot (Emsley et al., 2010) was used to perform the necessary steps needed to convert the datasets into 3D model structures of the proteins. This was done by first using the "Phaser-MR (simple one–component interface)" for the molecular replacement. Input files were the sequence file of the Cu-*Af*NiR, a pdb file of the already solved structure of Cu-*Af*NiR as a model, and the mtz-file from the data processing that is downloaded. This process creates a folder called Phaser which includes a new mtz, and pdb file. These are then used as input files together with the sequence file when "phenix.refine" is used to refine the data. Then follows a cycle of using Coot to manually model the structure, and refinement using phenix.refine. The changes in Coot consisted of using its functions like "Difference Map Peaks", "Unmodelled blobs", "Rotamer analysis", "Density fit analysis", and "Validation Outliers" to find areas in the model that did not fit the density in the best way. Some residues were then added or removed, some rotamers were rotated, as well as Cu atoms were inserted into the model. Water molecules and other molecules were also placed into the fitting blobs in the density map. The software PyMOL (Schrödinger, LLC, 2015) was then used to make the figures of the structures with the input files of the pdb file, density map file, and difference map file from the last refinement.

4 RESULTS AND DISCUSSION

The result in this thesis consists of crystal structures from the X-ray crystallization of Cu-NiR protein soaked in different solutions. The structures will first be displayed with their density map to showcase the fit of the structure and the experimental data. Selected active site structures of each Cu-NiR variant will then be compared to showcase the effect of the mutation and the soaking treatment. These structures will be more detailed. Analysis of the structures shows the mutated Glu98 and His 98 are coordinating the Cu atom in the Type-2 Cu active site in Cu-NiR. This creates novel active site variants with possibly new functions for the enzyme.

4.1 Protein Expression and Purification

Following the expression test (see Appendix) the glycerol stock used for expressing the mutants was colony 2 of Cu-NiR D98E and colony 3 of Cu-NiR D98H. These gave a similar amount of yield as the WT Cu-NiR, based on observation only.

4.2 X-ray crystallography

4.2.1 Protein crystallization

Following the results from the commercial screens used with sitting drop vapor diffusion crystallization, the conditions in which crystals grew were used for further optimization to find the optimal crystallizing conditions for the enzymes. The crystals obtained by crystallizing Cu-NiR are green, like soluble Cu-NiR protein (Figure 4.1). The biggest ones have clear-cut edges like a pyramid.
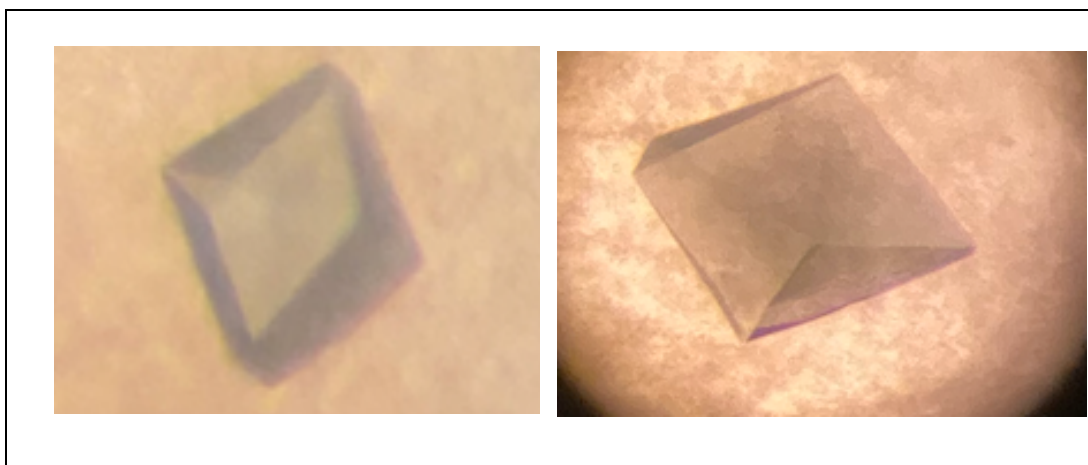
Figure 4.1. *Examples of Cu-NiR crystals in the microscope. They are green when saturated with Cu. Some of the crystals were big and easy to cryo-freeze, while others were smaller and more challenging to handle. Some precipitation around the crystals is visible.*

For the reduction of the crystals during the cryo-freezing, it was later discovered that the crystals should have been soaked in a reducing solution until they became colorless. Examples of this have taken one hour to complete. Given the limited space in the anaerobic work chamber, it was not possible to freeze the crystals in there. The reducing solution was therefore used surrounded by oxygen and would have trouble staying reduced for the full hour it would take to reduce the crystal (Murphy et al., 1997).

4.2.2 X-ray diffraction, data collection, and processing

The downloaded datasets for each processed crystal contained information about the processing including R_{merge}, Completeness, and Resolution. These can be found in the appendix. The highest resolution from each data processing pipeline with completeness above 90 % and as close to 100 % as possible was chosen to continue with molecular replacement and refinement. Tables of Crystal data, data collection, and refinements statistics for all structures are in appendix.

4.2.3 Structure Determination, refinement, and model building

Comparison of the three active sites in the same protein.

The structure of the three active sites may vary within the same protein. They are therefore shown side by side to showcase their similarities and differences. The following figures show the three type-2 Cu active sites, one from each monomer, from all the solved structures of *Af*NiR, with the density map and difference map made from the experimental data from the X-ray crystallization. The figures were prepared in PyMOL, using pdb-files, density-map, and difference-map from the last refinement of each structure. The following colors are used on all figures. The Nitrogen atoms are blue, the Oxygen atoms are red, and the carbon atoms are grey in the stick figures of the residues. The red spheres are water molecules, and the orange spheres are Copper atoms.

The density map is grey and set at level 2, while the difference map is red and green for the negative and positive differences, respectively, and set at level 3.

The following Table 4.1 show the structures solved by X-ray crystallography, as well as their soaking treatment, and some information about their active sites.

Table 4.1. *Overview of the solved crystals, divided by their amino acid number 98 in the solved structure, Asp for the WT, Glu for the D98E, and His for the D98H. Following is information about how many water molecules there are in the active sites, and the number of conformations amino acid number 98 shows in the density map, as well as the person the structure was solved by. AS = Anine Sætrang and EL = Eirin Landsem. Several numbers are separated by a comma where the active sites within the same structure have variations of numbers of water molecules or conformations of amino acids in the active sites. Note that there are two solved structures for reduced Cu-NiR WT without formate.*

* *One water molecule in two positions. Conf = conformation*

Cu-NiR variant	Redox condition	Added formate	Figure	Nr. of H_2O	Conf. of amino acid number 98	Solved by
WT	ox	No	Figure 4.2	1*	1	AS
WT	ox	Formate	Figure 4.3	0	2	AS
WT	red	No	Figure 4.4	2,1,1	1	AS
WT	red	No	Figure 4.5	1	1	EL
WT	red	Formate	Figure 4.6	2	1	EL
D98E	ox	No	Figure 4.7	0,1,1	1	AS
D98E	ox	Formate	Figure 4.8	1*	1	AS
D98E	red	No	Figure 4.9	1	1	EL
D98E	red	Formate	Figure 4.10	1	1	EL
D98H	ox	No	Figure 4.11	0, 1, 0	1	AS
D98H	ox	Formate	Figure 4.12	1	1	AS
D98H	red	No	Figure 4.13	1	1	EL
D98H	red	Formate	Figure 4.14	1	2,3,3	AS
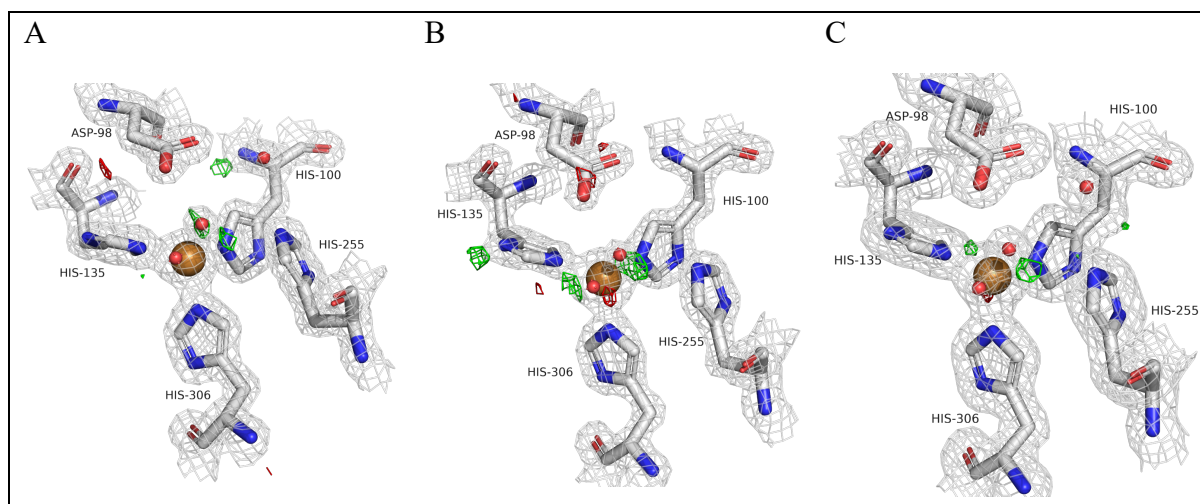
Figure 4.2. *Active sites in oxidized Cu-NiR WT without formate. There is only one conformation of the Asp98, and there are two water molecules modeled in each of the active sites. They represent one water molecule in two different positions. The occupancy of the water molecule is 0.68 and 0.32 for the two different positions.*

The three histidines His135, His306, and His100 are all coordinating Cu in the active site for all the Cu-NiR WT structures.
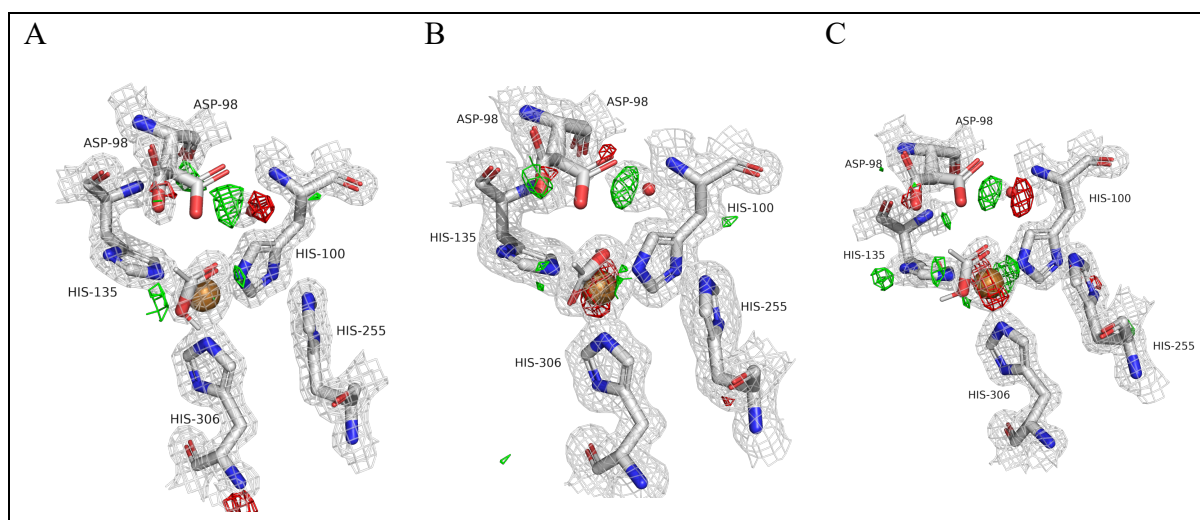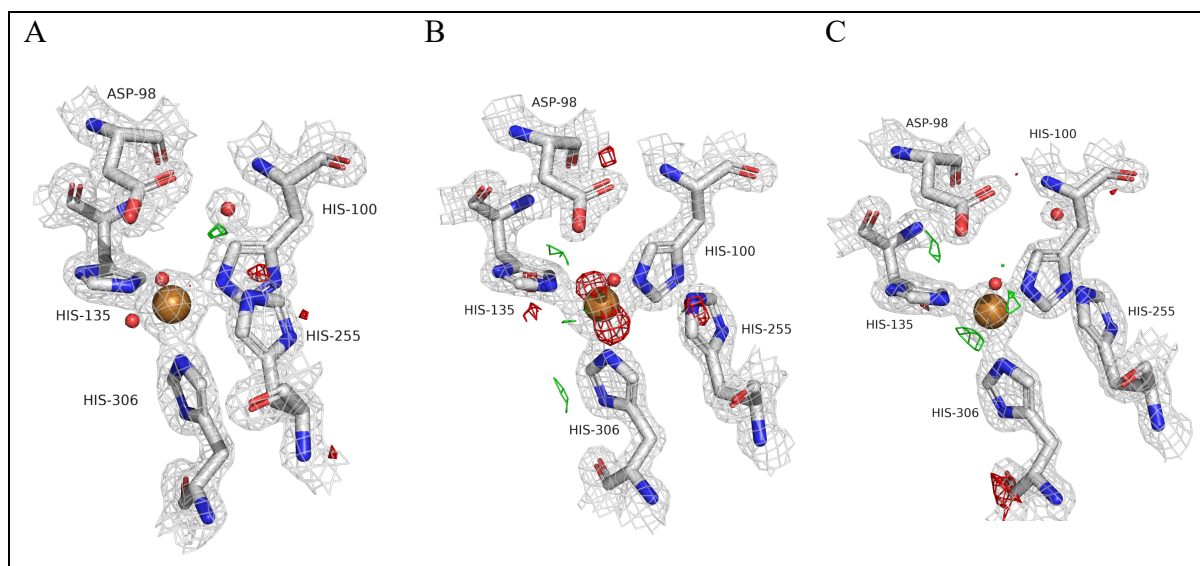

Figure 4.3. *Active sites in oxidized Cu-NiR WT with formate. One formate molecule is modeled in, at each of the active sites. Two conformations of Asp98 are shown in the density map.*

The structure in Figure 4.3 has a clear density for formate with occupancy of 76 %. The two conformations of Asp98, one pointing away from the active site and one pointing toward it, have an occupancy of 77 % and 27 % respectively. The similarities between the occupancy of formate at 76 %, and the occupancy of 77 % of Asp oriented away from the active site suggests that the Asp98 turns away from the active site to make room for the formate to bind. The 27 % occupancy of the conformation of Asp98 turned towards the active site will in this scenario be in the structures where there is no formate in the active site.

Similarly, (Tocheva et al., 2008) found two conformations for Asp98 modeled with 50 % occupancy each. However, it is suggested that the Asp98 conformation which is pointing towards the Cu is forming a hydrogen bond with the formate. This could indicate that the conformation pointing toward the Cu with 27 % occupancy in Figure 4.3 forms a hydrogen bond to formate which has an occupancy of 76 %. Tocheva et al. also found that two of the subunits in the structure showed two alternative binding modes for formate, one in which formate show bidentate coordination with both of its oxygens and another where formate showed monodentate weaker binding with only one oxygen. This alternative monodentate binding mode of formate was not observed in our data (Figure 4.3).

Figure 4.4. *Active sites in reduced Cu-NiR WT without formate. Two water molecules are modeled in active site A, while only one water molecule is modeled in active sites B and C. Only one conformation of Asp98 is shown in the density map. This crystal was soaked in solution 2A. which was made by purging reservoir solution with N₂ outside the anaerobic chamber and adding DT to the solution in the anaerobic chamber. A vial with a septum was used to keep the solution reduced.*

27

The crystal used to find this structure was soaked in reducing conditions, but it seems the enzyme was not fully reduced. A reduced structure in (Murphy et al., 1997) is shown as having no other water molecule in the active site other than the one coordinating Asp98 and His255.
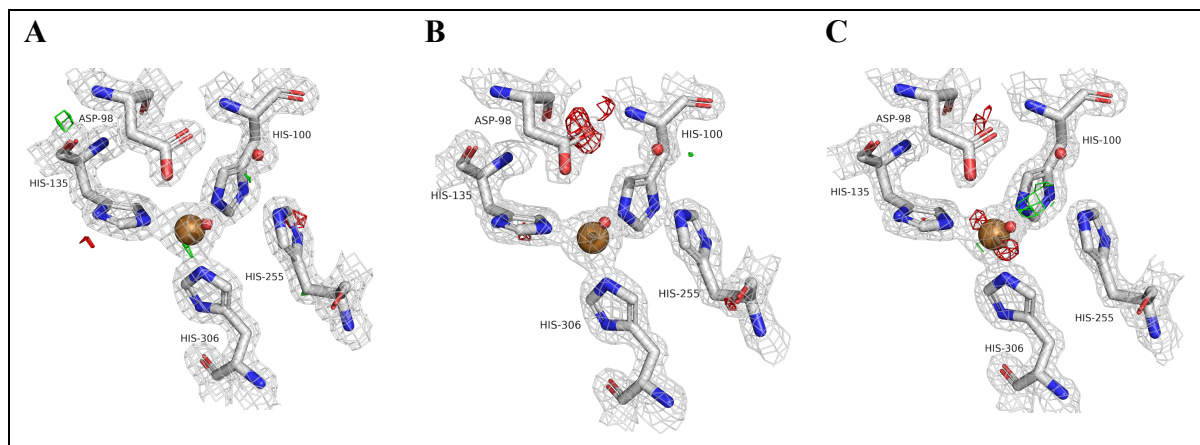
Figure 4.5. Active sites in reduced Cu-NiR WT without formate. One water molecule is modeled in each of the three active sites. One conformation of Asp98 is shown in the density map. This crystal was soaked in solution 2B which was made with reservoir solution purged with N2, 2 mg DT, and 6.8 mg formate left in the anaerobic work chamber overnight before it was mixed in a vial with a septum.

Figure 4.4 and Figure 4.5 are both reduced Cu-NiR WT without formate. They were reduced in different ways, in an effort to compare several reducing methods. Figure 4.4 was reduced with solution 2A, and Figure 4.5 was reduced with solution 2B. While Figure 4.4 has one active site containing two water molecules and two active sites containing one water molecule, Figure 4.5 has only one water molecule in all three active sites.
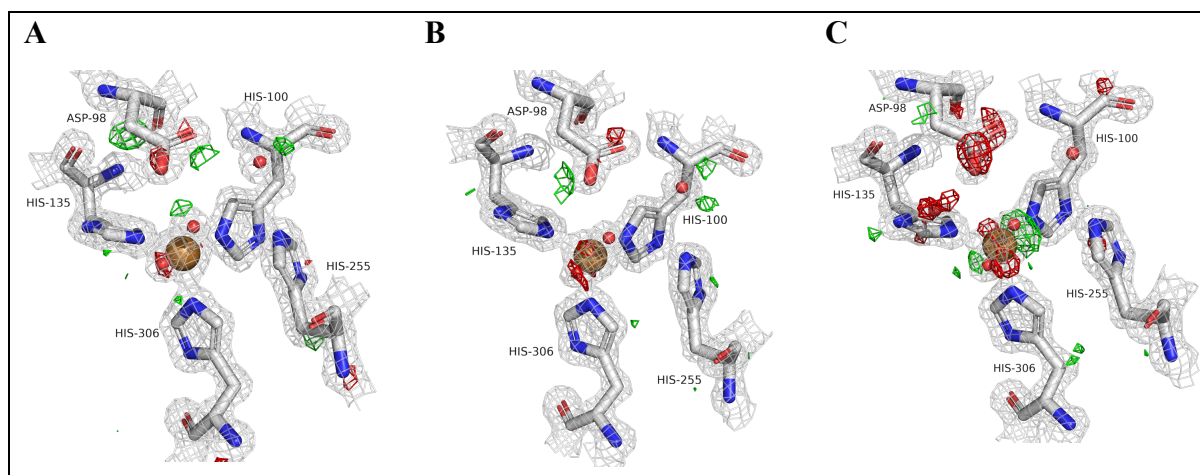
Figure 4.6. *Active sites in reduced Cu-NiR WT with formate. Two water molecules are modeled in each of the active sites. One conformation of Asp98 is visible in the density map.*

Formate, CO, and NO were all tested in the density, but none of them fit and resulted in significant difference map peaks compared with the two water molecules at 100% occupancy each. Although the crystal was soaked in formate, it does not contain formate.
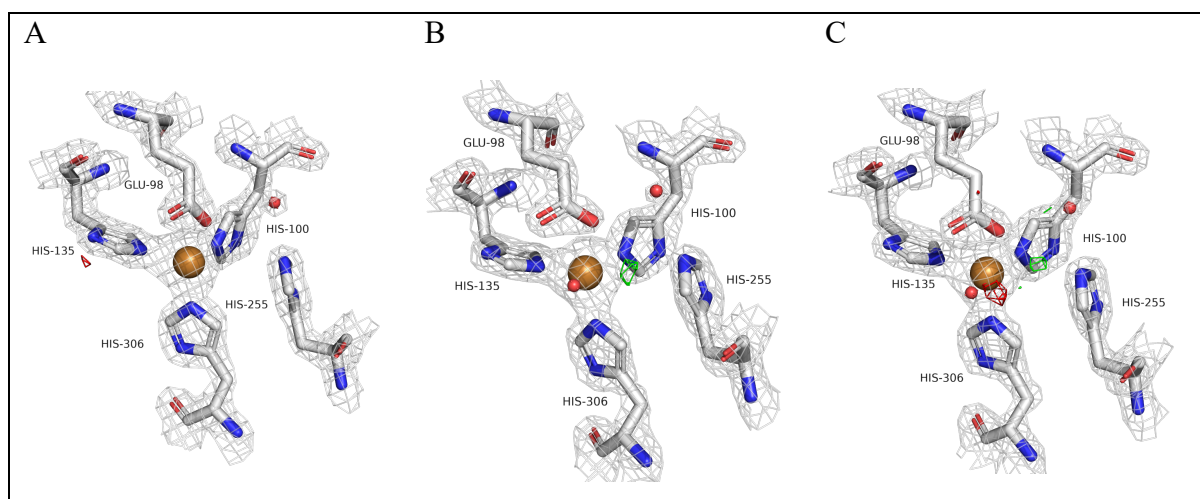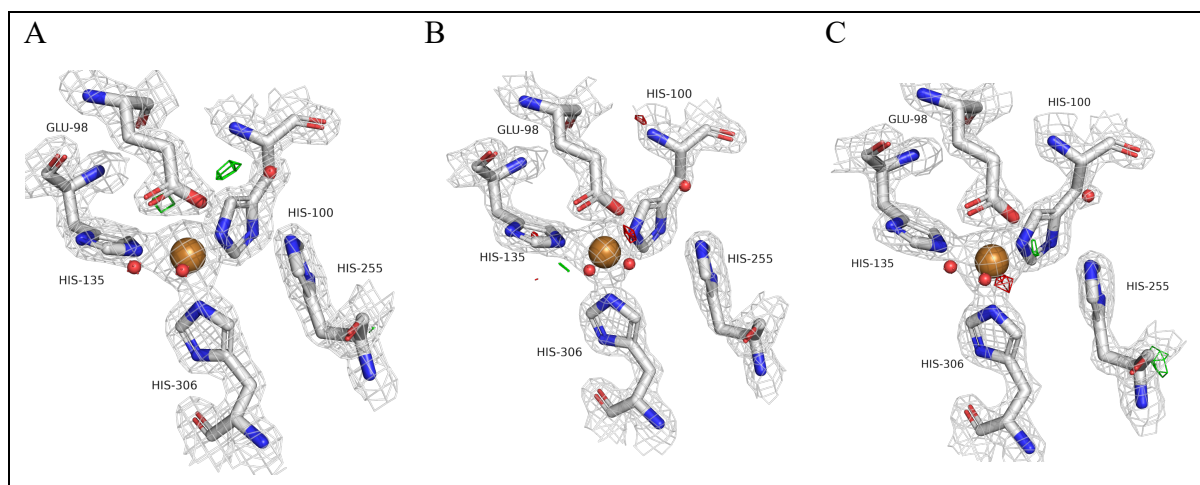

Figure 4.7. *Active sites in oxidized Cu-NiR D98E without formate. There are modeled one water molecule in the active sites B and C, but none in active site A. There is only one conformation of Glu98, and it coordinates with the Cu atom in the same way as His135, His306, and His100 do.*

The histidines His135, His306, and His100 is coordinating the Cu in the active site in the Cu-NiR D98E structures as well as the WT structures. In addition, Glu98 is also coordinated with

Cu. A new active site is created by mutating Asp98 to Glu98. This could be affecting the function of the enzyme.


Figure 4.8. *Active sites in oxidized Cu-NiR D98E with formate. The active sites have one water molecule in two alternative positions. One of the positions is close to Cu, 2.1Å, and another a little further from Cu, 3.8 Å, measured in structure A. There is only one conformation of Glu98, also coordinating the Cu atom.*

Formate was modeled in but did not fit the density, indicating that soaking this crystal in a solution containing formate did not make the D98E mutant bind formate in the Type-2 Cu active site. The bigger size of the Glu98 in the D98E mutant compared to the WT, as well as their different positions and pK$_a$ might be causing the formate to not bind in the active site. Glu98 is also creating a new active site variant by coordinating the Cu atom.
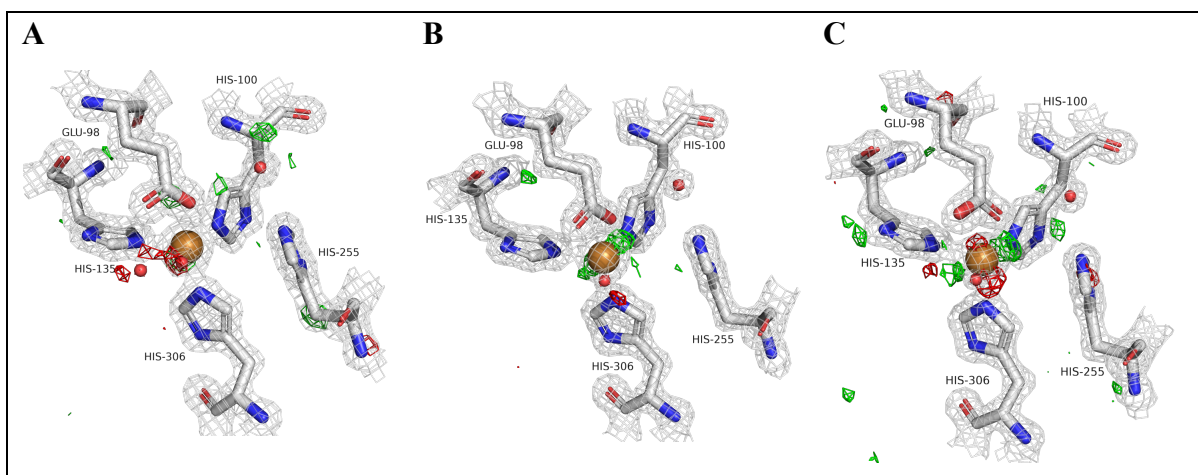
Figure 4.9. *Active sites in reduced Cu-NiR D98E without formate. One water molecule is modeled in all three active sites, and there is only density for one conformation of Glu98. The Glu98 is coordinating the Cu in the active site.*
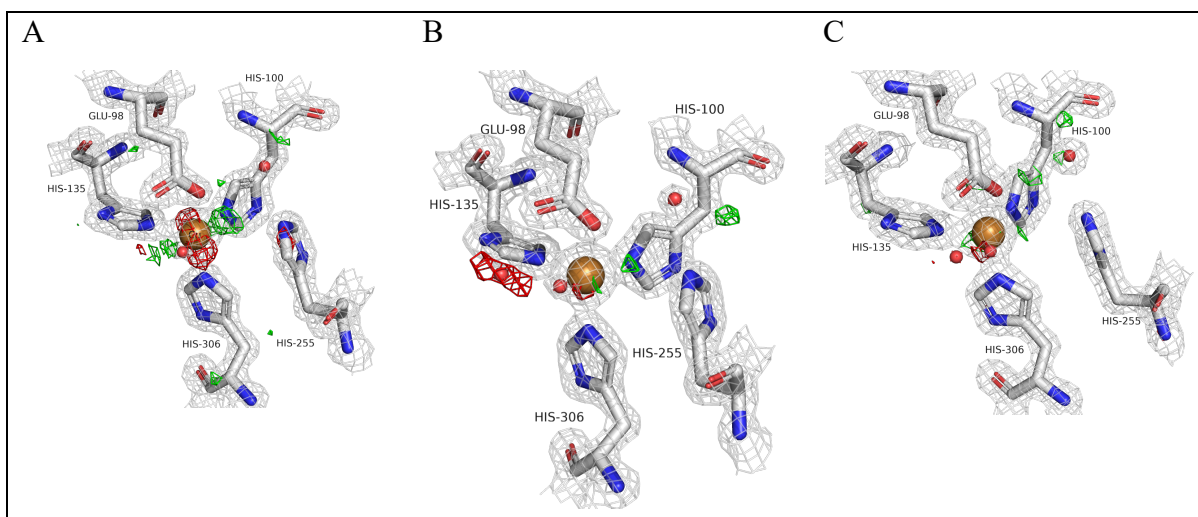
Figure 4.10. *Active sites in reduced Cu-NiR D98E formate. There is one water molecule in each of the three active sites, and there is only one conformation of Glu98. The Glu98 is coordinating the Cu, as the histidines are.*

There is no density to put formate in, and since there is density for a water molecule in the active site, it seems the protein was not fully reduced (Murphy et al., 1997).
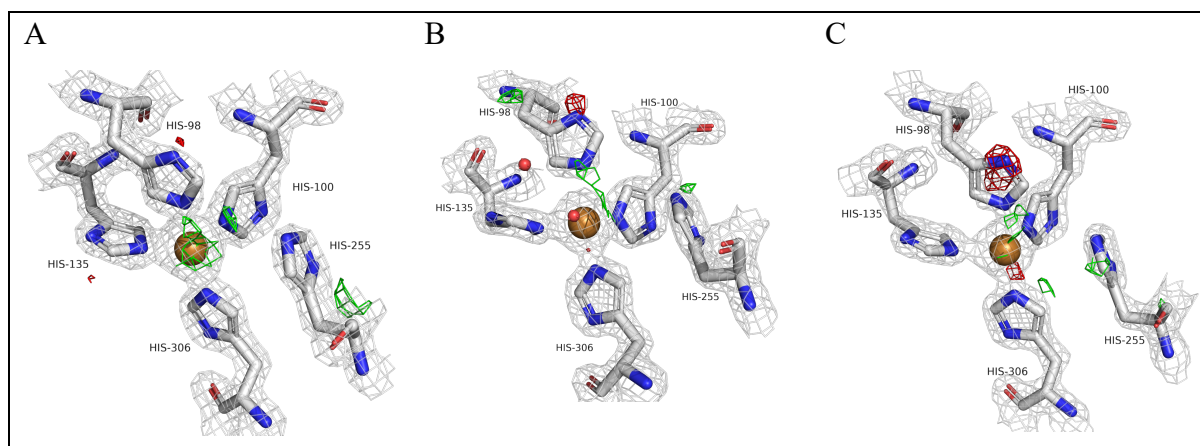
Figure 4.11. *Active sites in oxidized Cu-NiR D98H without formate. Active site B is the only one that has one water molecule modeled, and there is only one conformation of His98 in all three active sites. His98 coordinates to Cu as the other histidines do. This may cause new functions of the enzyme.*

As seen in the Glu98 structures, His98 is also coordinating the Cu atom in the active site, like the histidines His135, His306, and His100 are. This is creating another active site variant with possible new functions.
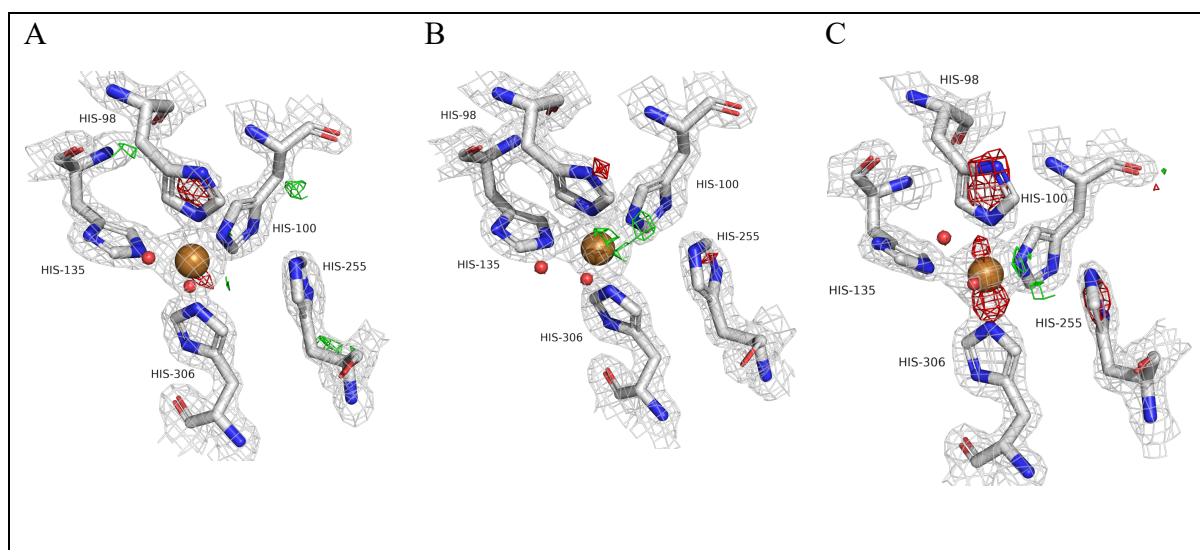
Figure 4.12. *Active sites in oxidized Cu-NiR D98H with formate. All three active sites have one water molecule modeled in the active site, and another a little further away by the His135 residue. There is only one conformation of His98, which is also coordinating the Cu atom.*

There is no density for formate in the active site in Figure 4.12, so it seems the soaking in formate was not successful at binding formate in this structure.
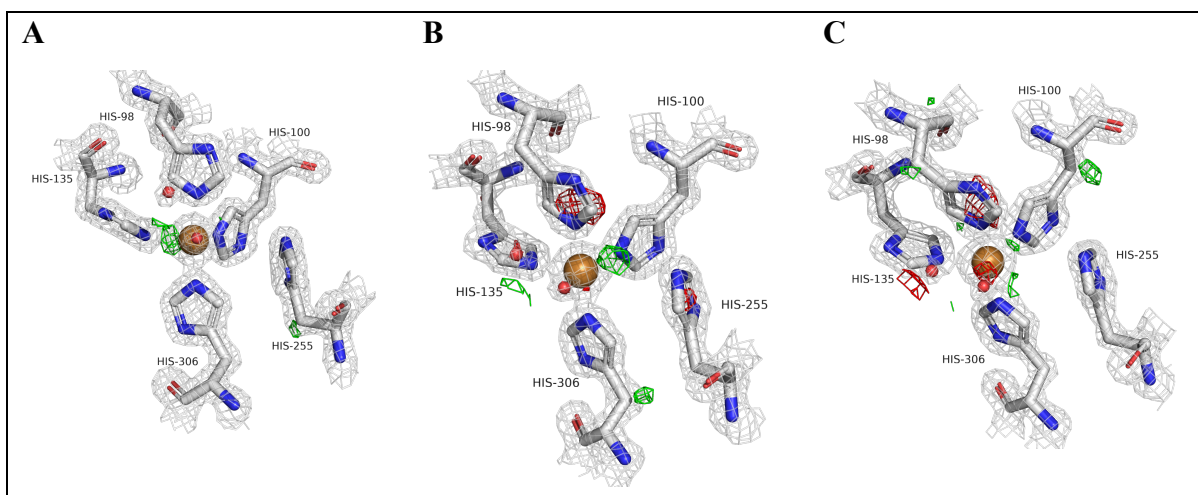
Figure 4.13. *Active sites in reduced Cu-NiR D98H without formate. There is modeled one water molecule in each of the three active sites, and there is only one conformation of His98. Along with the other His98 structures, this structure also has His98 coordinating the Cu atom in the active site.*

In Figure 4.13 there is density for one water molecule in each of the active sites, suggesting it is not fully reduced.
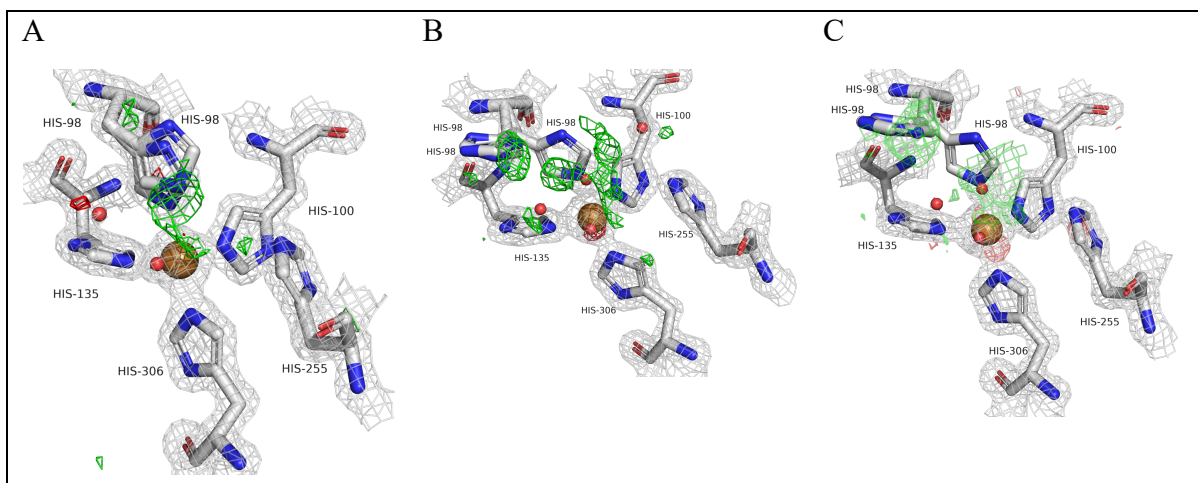
Figure 4.14. *Active sites in reduced Cu-NiR D98H with formate. There is only one water molecule modeled in each of the active sites, but there are several conformations of His98. In active site A, there are two different conformations, while there are three in B and C. The confirmations that are pointing toward the active site are coordinated with the Cu atom.*

There is no density for formate in reduced Cu-NiR D98H with formate (Figure 4.14), meaning the soaking in a solution containing formate was not successful at binding formate in the protein. Active site A shows two conformations of His98, and active sites B and C show three conformations of His98. The His98 conformations that are pointing towards the active site, are coordinating the Cu atom.

Comparison of the structures.

One of the active sites from each structure has been chosen to represent the structure, as they are compared to each other based on the number of water molecules, distances, conformations, and placement of the amino acid number 98, and their reduction. The density map has been removed for clarity, as have the backbone of the residues. Water molecules and residues are labeled, and some selected distances are shown. Other selected distances are noted in the text. While the visual, and measured structure is a result of experimental data, the interpretation of them is largely based on an attempt to find patterns and logic within the structures, as well as comparing them to existing structures. While the structures are named after their soaking conditions, it is noted in the discussion that the soaking was not always successful. Reducing the enzyme was especially a challenge, as well as binding formate to the mutated enzymes. Even though the soaking was not always successful, the active sites have still been affected in several structures.

Cu-NiR WT structures compared.
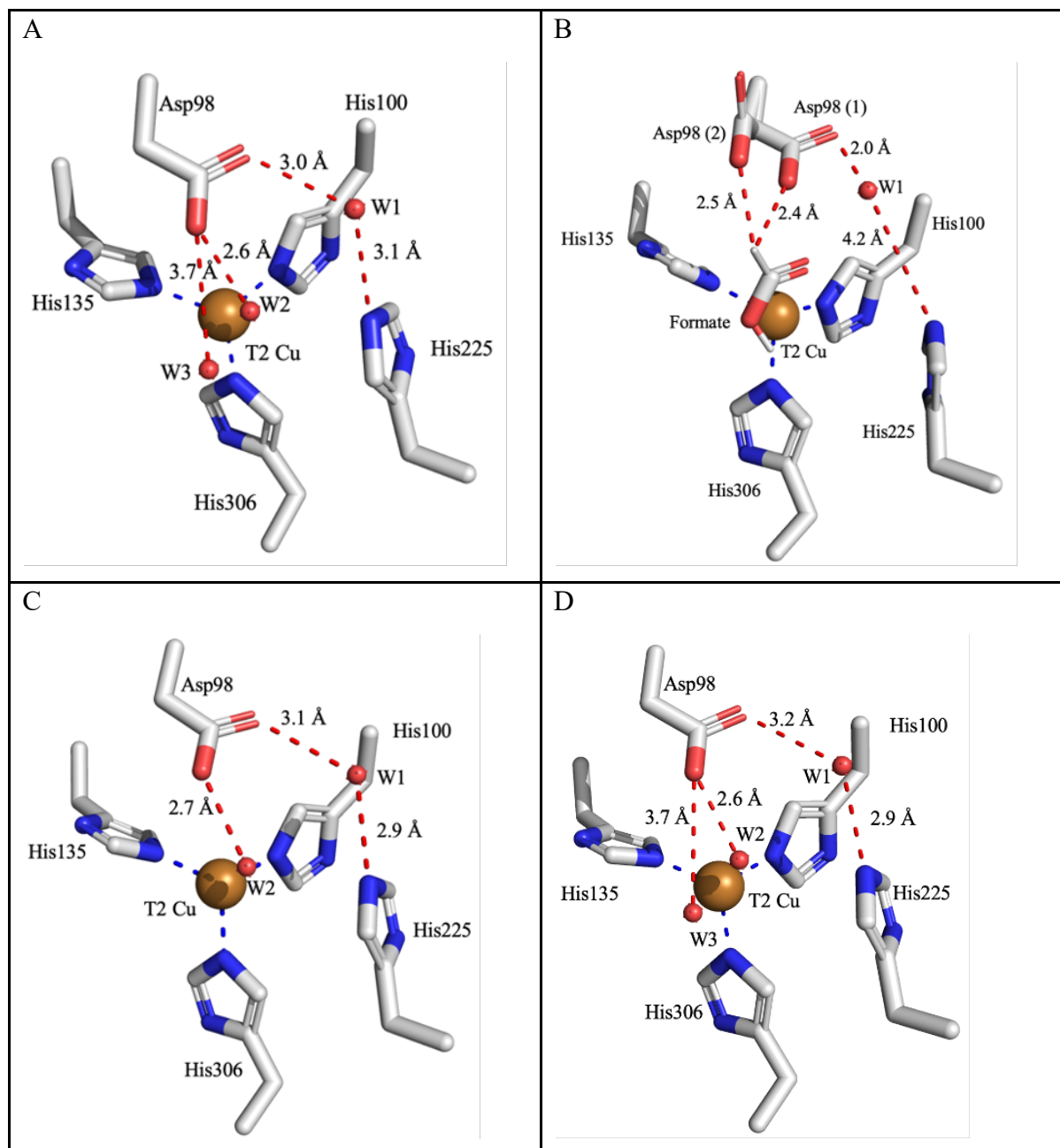
Figure 4.15. *Key active site residues from Cu-NiR WT crystals with different soaking treatments, A)*
oxidized without formate, B) oxidized with formate, C) reduced without formate, and D) reduced with
formate. The histidines His135, His306, and His100 are all coordinated by the Cu atom. The differences
between these structures are the number of water molecules in the active site, and slightly different
distances between the W2 and Asp98 in A, C, and D. B is quite different from the others as it contains
formate in the active site. This also affects the distances between W1 and the coordinating amino acids
Asp98 and His225. A has two water molecules, W3 and W2, 3.7 Å and 2.6 Å away from Asp98,

respectively. B has one formate modeled in the active site at 76 % occupancy, 2.5 Å and 2.4 Å away from Asp98 (2) and Asp98 (1) respectively. C contains one water molecule at a 2.7 Å distance from Asp98. D has two water molecules W3 and W2 at 3.7 Å and 2.6 Å distance from Asp98 respectively. The distances from Cu to the two water molecule positions in A are 2.4 Å for W3 and 2.2 Å for W2. The distances from Cu to formate in B are 2.2 Å and 2.3 Å to the oxygen atoms and 2.5 Å to the carbon atom. The distance from Cu to W2 in C is 2.3 Å. The distance from Cu to W3 and W2 in D is 2.2 Å and 2.3 Å respectively. The distance between Asp98 and W1, and W1 and His225 are also different in B compared to the others, with 2.0Å and 4.2 Å respectively. A, C, and D all have 3.0-3.2 Å and 2.9-3.1 Å from Asp98 to W1, and W1 to His225 respectively.

The distance from Asp98 to W1 is 3.0 Å, 3.1 Å, and 3.2 Å in A, C, and D respectively. The distance from W1 to His225 is 3.1 Å, 2.9 Å, and 2.9Å in A, C, and D respectively. B is different from the others as the distance from Asp98 to W1 is 2.0 Å and the distance from W1 to His225 is 4.2 Å. This seems to be the result of the two different conformations of Asp98 which is altering the hydrogen bonding network in the active site. B is also the only structure with formate in the active site, suggesting that the formate is causing the change in structure for the Asp98 and the water molecule W1.

For the oxidized Cu-NiR WT without formate in A in Figure 4.15, other studies have found that one water molecule is placed this close to the Cu atom at the Type-2 Cu active site in *Af*NiR (Murphy et al., 1997). As discussed in Figure 4.2 there is one molecule with two different conformations in Figure 4.15 A. Both A and D have two water molecules (position for A) W3 and W2 at the same 3.7 Å and 2.6 Å distance from Asp98 respectively. They also have similar distances between Asp98, W1, and His225. While A is oxidized without formate, D is soaked in reducing conditions with formate. This indicates that D was not fully reduced and does not contain formate as was intended by the preparation of the crystal before the X-ray crystallography. It is therefore unknown whether the fully reduced protein will bind formate with the methods described in this thesis.

The reduced crystals did not become colorless, suggesting the enzyme was still oxidized. The reduced structure should also not have water molecules coordinated to the Cu in the Type-2 Cu site as seen in this structure (Murphy et al., 1997). The reducing soaking conditions have however affected the active sites when it comes to the number of water molecules, even though it should ideally not be any water molecules in the reduced structures. The structures from Figure 4.4. and Figure 4.5 are both reduced Cu-NiR WT without formate, but they are reduced

36

with solutions 2A and 2B respectively. There are still water molecules in the active site in both structures, suggesting the protein was not fully reduced, but there are fewer water molecules in the crystal soaked in solution 2B, indicating it might have been better at reducing the protein. Given the fact that the crystals were soaked for less time in solutions 2B and 3B, than in solutions 2A and 3A, it seems it was a better method of creating the reducing solution.

The distance from the water molecules in the active site to the Cu is an indicator of possible open coordination sites in the metal. The distances shown in the WT are all 2.4 Å or below and might indicate such an open coordination site.

Cu-NiR D98E structures compared.
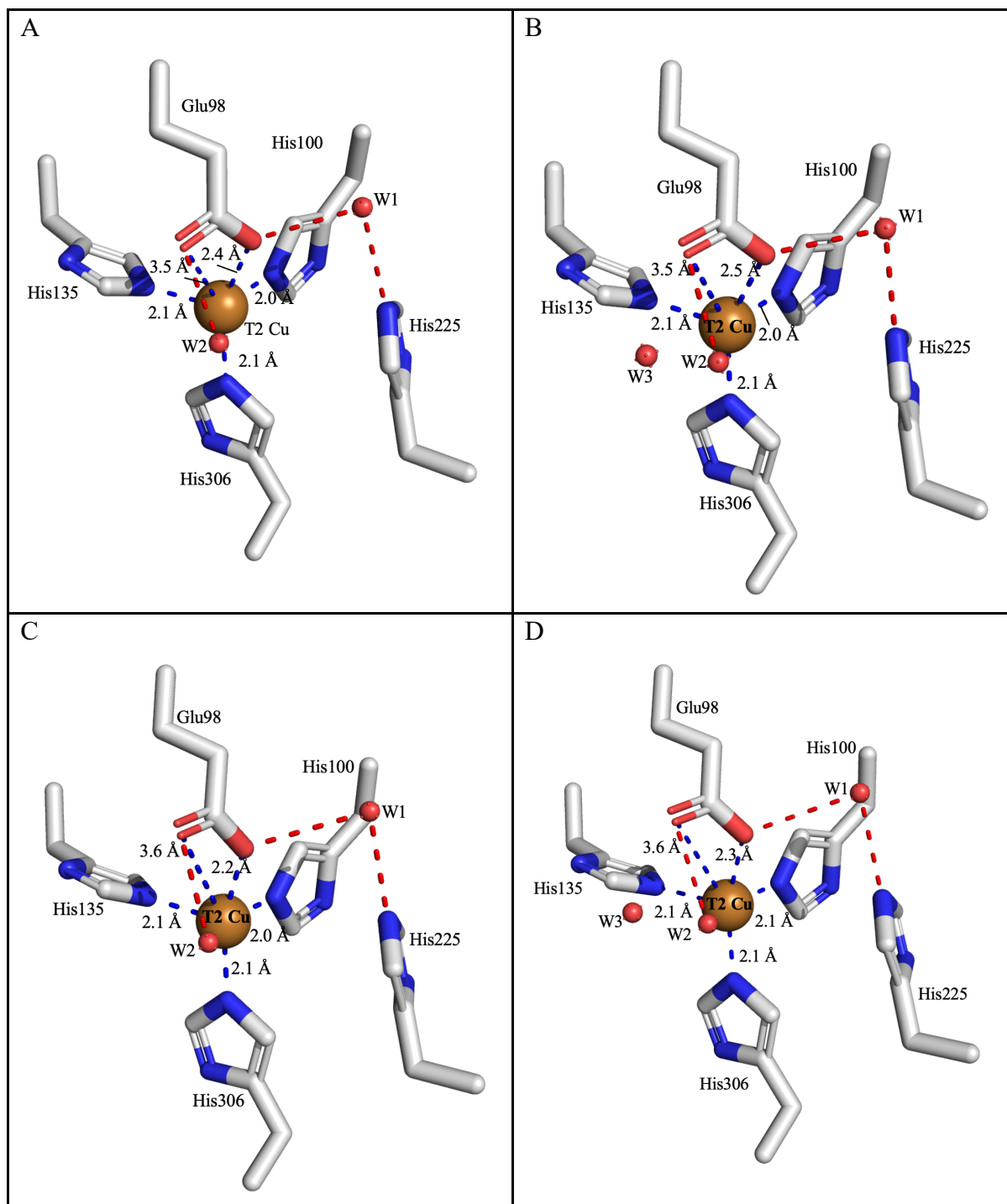
Figure 4.16. *Key active site residues from Cu-NiR D98E crystals with different soaking treatments, A) oxidized without formate, B) oxidized with formate, C) reduced without formate, and D) reduced with formate. The histidines His135, His306, and His100 are coordinating the Cu in the same way as they are in WT Cu-NiR. His135 and His306 both have 2.1 Å to the Cu in all the D98E structures, while*

His100 has 2.0 Å to the Cu in A, B, and C. His100 has 2.1 Å to the Cu in D. The mutation of Asp98 to Glu98 causes this amino acid to also coordinate with Cu. They are visualized by blue lines like the histidines. The distance from the oxygen atoms in Glu98 to Cu is from left to right 3.5 Å and 2.4 Å in A, 3.5 Å and 2.5 Å in B, 3.6 Å and 2.2 Å in C, and 3.6 Å and 2.3 Å in D. Both A, C, and D have one water molecule (W2) at the distance of 2.8 Å from Glu98, while B has 2.9 Å between Glu98 and the W2 water. The distance from Cu to W2 is 2.1Å in A and D, but 2.2 Å in C. In B there is one water molecule with two possible conformations in the active site and the distance from Cu to W2 is 2.1 Å, while the distance from Cu to W3 is 3.8 Å.

There is a distinctive difference between how close the Asp98 in the WT and the Glu98 in D98E are to the Cu- atom, the Glu98 being a lot closer. The distance between Asp98 and the Cu in oxidized Cu-NiR WT without formate is 3.8 Å and 4.7 Å, while the distance between Glu98 and the Cu in oxidized Cu-NiR D98E without formate is 3.5 Å and 2.4 Å for each of the two oxygen atoms. This might affect the amount of space there is in the active site for molecules to bind. The limited space for substrate binding in the active site caused by mutating Asp98 to a longer amino acid, Glu98, might cause difficulty in binding formate in the active site. It seems that Glu98 is directly coordinated with Cu, creating a novel active site variant of Cu-NiR. This is similar to Figures 3 b and c in (Ellis et al., 2003).

Two water molecule conformations in the active site of B, oxidized Cu-NiR D98E with formate, differ from the oxidized Cu-NiR D98E without formate in A. Figure 4.7 shows that the oxidized Cu-NiR D98E without formate only has one water molecule in two of the active sites. Although oxidized Cu-NiR D98E with formate in Figure 4.8 was soaked in conditions where formate could have been introduced to the active site, it seems like that did not occur. It can therefore be considered to be similar to the oxidized Cu-NiR D98E- without formate structure (Figure 4.7), but it is important to note the difference in the position of the water molecule in their active sites. This might be a result of the attempt to add formate to this structure. There is no indication of Glu98 having more than one conformation and therefore giving space for formate binding as seen in the oxidized Cu-NiR WT with formate in Figure 4.3. The longer amino acid Glu might have a harder time flipping compared to the shorter Asp in the WT.
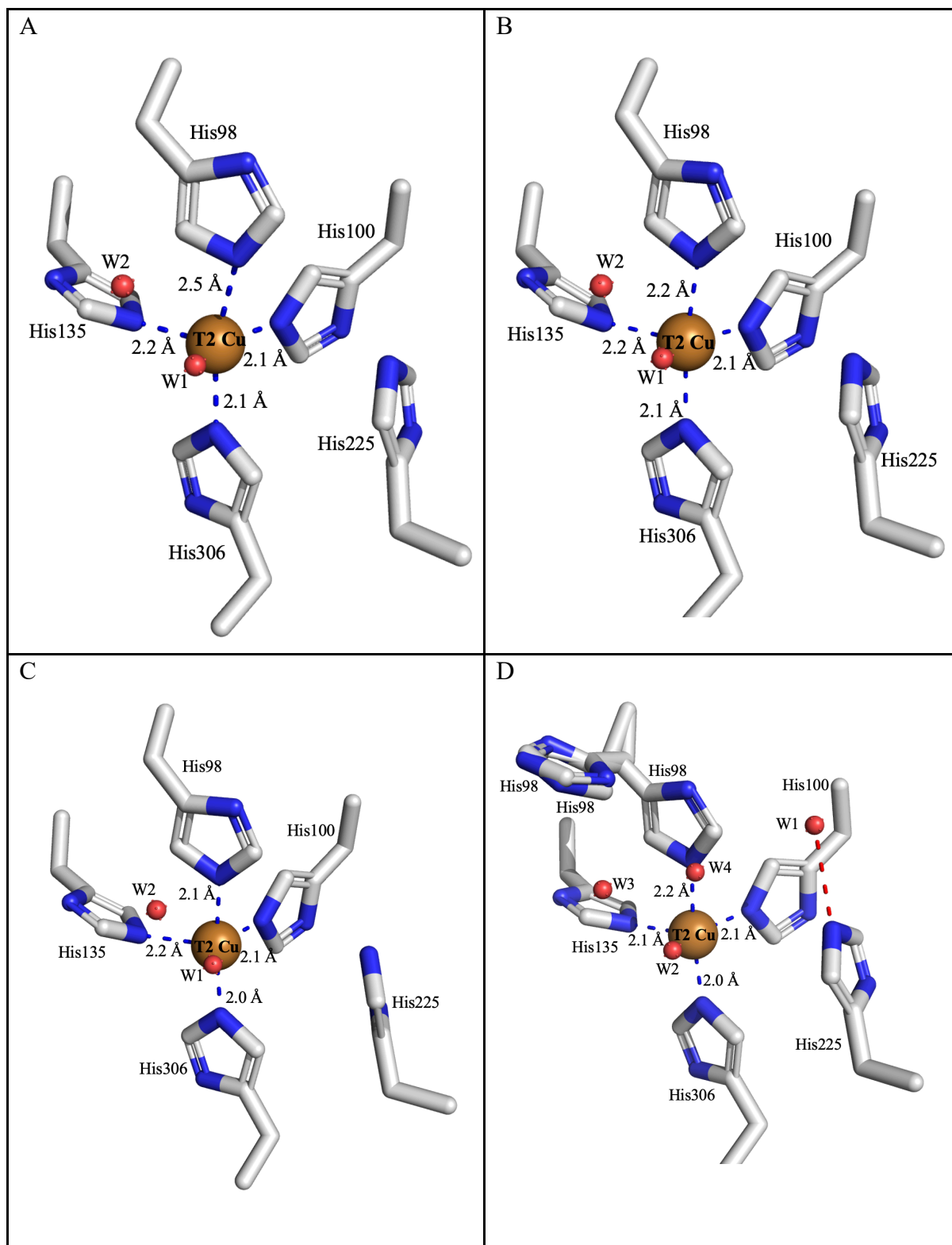
Active sites in reduced Cu-NiR D98E without formate, Figure 4.16C, is similar to the reduced Cu-NiR WT without formate crystals with Figure 4.5 having one water molecule in each of the active sites and Figure 4.4 having one water molecule in two of its active sites. Figure 4.16 C was like Figure 4.5 soaked in solution 2B to be reduced and the proteins have the same amount of water molecules in their active sites. It seems it is not fully reduced, as the crystal was not colorless when frozen, and there are water molecules in the active site (Murphy et al., 1997).

While the reduced Cu-NiR WT with formate in Figure 4.15 D has two water molecules modeled in each of its active sites, there is only one water molecule in each of the active sites in reduced Cu-NiR D98E with formate in Figure 4.10They were both soaked in solution 2B, so the only difference between them is the mutation in amino acid number 98. The Glu98 is bigger than Asp98 and that might affect the number of water molecules that can bind in the active site.

The distances from Cu to the W2 water molecules in the active site are 2.2 Å or below for all the structures. This could indicate an open coordination site for the Cu metal. The Cu is already coordinating three histidines and the Glu98 in these structures. Another coordination site could make room for other potential chemical reactions.

Cu-NiR D98H structures compared.

Figure 4.17. *Key active site residues from Cu-NiR D98H crystals with different soaking treatments, A) oxidized without formate, B) oxidized with formate, C) reduced without formate, and D) reduced with*

41

formate. His135, His306, and His100 are coordinating the Cu as they do in WT Cu-NiR. The distance from His135 to Cu is 2.2 Å in A, B, and C, but 2.1 Å in D. The distance fromHis306 to Cu is 2.1 Å in A and B, but 2.0 Å in C and D. The distance from His100 to Cu is 2.1 in all the structures. It seems the His98 is directly coordinating the Cu, like the other histidines. The distance between the His98 and Cu shown in A is 2.5 Å, in B it is 2.2 Å, in C it is 2.1 Å, and in D it is 2.2 Å. The His98 is therefore mostly as close as the other histidines bound to Cu. The water molecule that is marked as W1 in all the Cu-NiR WT and D98E structures, is coordinating the His225 and the proton donating amino acid Asp98 in the WT. It is only present in D in Cu-NiR D98H and is not modeled in A, B, and C. The distance from Cu to W1 is 2.0 Å in A, B, and C. In D the distance from Cu to W2 is 2.2 Å.

The His98 seems to be directly coordinating the Cu in all the structures, as it is mostly the same distance away from Cu as the other coordinating histidines. This affects the geometry, structure, and likely activity of the enzyme. It creates a novel active site variant of copper-dependent nitrite reductase from *Alcaligenes faecalis* with D98H mutation.

Compared to the oxidized Cu-NiR WT without formate in Figure 4.2, which contains one water molecule with two conformations in each of the active sites, and oxidized Cu-NiR D98E without formate in Figure 4.7, in which two of the active sites contain one water molecule, the oxidized Cu-NiR D98H without formate in Figure 4.11 has the least water molecules. This might be caused by the His being a bigger amino acid because of the ring structure. There is possibly simply less space in the active site for substrates to bind.

It seems the soaking in formate was not successful at binding formate in any of the Cu-NiR D98E and D98H structures. Only oxidized Cu-NiR WT with formate in Figure 4.3 contains formate after being soaked in it. They were all soaked in the same solution during cryofreezing, so the only difference between these crystals is their mutation in amino acid number 98. The D98E and D98H mutants have bigger amino acids than the WT Asp98 which seems to affect the enzymes' ability of binding formate in an oxidized state. None of the crystals soaked in reducing conditions containing formate has formate bound to their active sites. As the reducing conditions were not fully successful, it is not certain if that influenced the binding to formate, but the mutants did not bind formate in an oxidized state even though the WT did.

Comparing oxidized Cu-NiR D98H with formate to oxidized Cu-NiR D98H without formate in Figure 4.11, where only one of the active sites has one water molecule, it seems again that

42

there are more water molecules in the structures of oxidized mutant-NiR that have been soaked in formate. The same effect is seen in oxidized Cu-NiR D98E without formate Figure 4.7 where two active sites have one water molecule and in oxidized Cu-NiR D98E with formate in Figure 4.8 where each active site has two water molecules. Although the attempt at introducing formate into the active sites of the mutants D98E and D98H was unsuccessful, the active sites contain more water molecules when the crystals have been soaked in a solution with formate so there is a change in the structure.

Active sites in reduced Cu-NiR D98H without formate have a density of one water molecule in each of the active sites. This is similar to reduced Cu-NiR D98E without formate in Figure 4.9 reduced Cu-NiR WT without formate in Figure 4.5, and two of the active sites in reduced Cu-NiR WT without formate in Figure 4.4, which all contain one water molecule in the active site. Active sites in reduced Cu-NiR D98H with formate contain one water molecule in each. This is similar to reduced Cu-NiR D98E with formate in Figure 4.10, which also contains one water molecule in each of its active sites. All of the crystals that were soaked in reducing conditions, contain water molecules in their active sites, suggesting that they are not fully reduced, in line with their not colorless crystal after the soaking (Murphy et al., 1997). Since there is no difference in the number of water molecules in the active sites between the reduced mutants Cu-NiR D98E and D98H soaked in formate, it is not certain if the different conformations in D98H influence the active site.

The distance from Cu to the W1 water molecules in A, B, and C is 2.0 Å and from Cu to W2 in D the distance is 2.2 Å. This could indicate another open coordination site in Cu, which could have possibilities for unknown chemical reactions.

Observed patterns.

Because the number of water molecules in the active site sometimes varies within the same structure, it is not simple to find a pattern. Also, because of the uncertainty of the success of the soaking conditions for a lot of the crystals, the effect of the soaking is discussed but not concluded. For the oxidized mutants, the number of water molecules and their position in the active site differ if they were soaked in formate, even if they did not bind to formate. For the reduced mutants there is not a lot of difference between the ones soaked in formate or without formate.

The only structure containing density for the formate, oxidized Cu-NiR WT with formate, has an occupancy of formate at 76 %. It also has two conformations of Asp98 with the one pointing away from the active site and the formate having an occupancy of 77 %, while the conformation pointing toward the active site has an occupancy of 27 %. It is suggested that the change in conformation or anisotropy of the amino acid is vital for the binding of formate in the active site. The residues on the surface of proteins are freer to have more conformations, meaning they are often anisotropic (Eyal et al., 2007). The coordination of Cu-NiR is tetrahedral with the histidines and the coordinating water molecule between Asp98 and His225. This geometry was clearly changed in the oxidized Cu-NiR WT with formate. The change in the geometry of the coordinating water molecule between Asp98 and His225 might affect the proton donation in the nitrite reduction.

The mutants seem to take too much space in the active site, not giving room for the formate to bind. They, therefore, seem to act as inhibitors for enzyme activity. In the WT the Asp98 is small enough to make room for the formate to bind, while in the mutants D98H and D98E, it will not bind. It also seems like Glu98 and His98 are directly coordinating Cu, resulting in novel active site variants of Cu-NiR. Since formate is similar to nitrite, it is possible that the mutations will act as substrate-binding inhibitors. This would have to be confirmed with an activity assay. The lack of binding of formate in the active site of D98E and D98H does not exclude the possibility of them catalyzing CO_2 reduction. As formate is the product of reducing CO_2, it is not necessary for it to be able to bind to the enzyme. Only the substrate must be able to bind to the enzyme, creating a substrate-enzyme-complex.

Nitrite reductase with other transition metals in the active sites.
Purified *Af*NiR was saturated with Ni in an attempt to make crystals with Ni in the active site. Some of these crystals were grown in conditions containing Co, making it possible that Co was inserted in the activity site. The structural data of these crystals showed that this was not the case.

Possible Nir with D98H in nature.

Searching through sequence databases and using alpha fold, has provided examples of possible Nir-enzymes in nature containing His98. One example with UniProt ID A0A069DG28 is shown in Figure 4.18 It is not proven what function these enzymes might have in nature, but the large number of them is interesting. This is also only an automatic search; more manual searching might find even more of these sequences. This also gives more insight into why the D98H mutation was chosen for this project, as the variant in nature may have a function. The variant of the active site might change the enzyme's redox potential and catalytic ability. However, it does not prove anything of this enzyme's possible new activity.
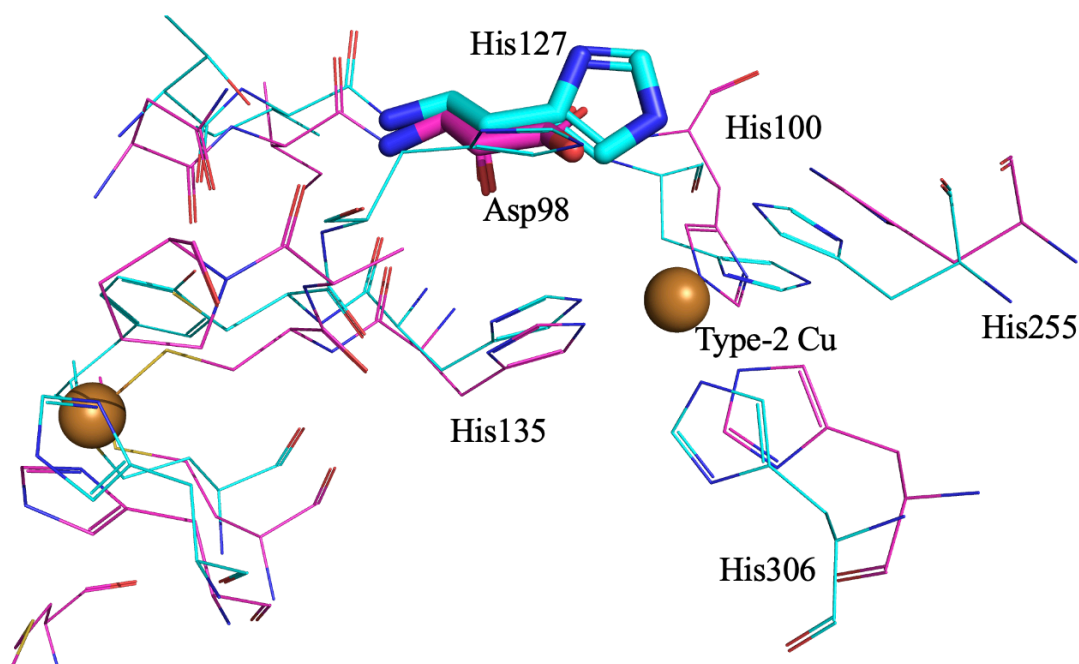
Figure 4.18. *One example of one D98H variant found in nature in blue, shown together with the WT variant in purple. The variant with Histidine in the proton donor position displayed here has UniProt ID A0A069DG28, and the WT structure has PDB ID 5F7B. The structures are similar but with the variant of His instead of Asp98.*

5 CONCLUSIONS AND FURTHER PERSPECTIVES

The structures suggest that the mutation of Asp98 into Glu98 and His98 in Cu-NiR was successful, as they both fit the density- map from the X-ray crystallization. None of the mutants has density for formate in their structures, while the WT has density for formate at 76 % occupancy. The mutated amino acids Glu98 and His98 also seem to be directly coordinating Cu, creating novel active site variants of copper-dependent nitrite reductases. This has the possibility to alter the function of the enzyme. The distances from Cu to the water molecules in the active site in both mutants could indicate open coordination sites for Cu.

Cu-NiR D98H possibly existing in nature is interesting beyond the COOFIX project, as there is no knowledge of what this mutant is involved in. Although it might not be reducing CO_2 to formate, the enzyme might be useful in other reactions.

The crystals were not fully reduced, as they did not become colorless in the reducing condition solution. However, some of the structures are different from the oxidized ones, so they have been affected by the reducing condition and are possibly partially reduced. Reducing the crystals for a full hour until they are colorless will be the next step in working with these crystals.

As the WT is able to bind formate, other mutants might also be able to. The ability of the enzyme to bind formate is also not an indication of its ability to reduce CO_2. As formate is the product of CO_2 reduction, it is not necessary for it to bind to the enzyme. The possibility for the enzymes to reduce CO_2 to formate can be tested in an activity assay. An activity assay for proteins to research if they are able to reduce CO_2 to formate is currently in the works by the COOFIX – project.

REFERENCE LIST

Afonine, P. V., Grosse-Kunstleve, R. W., Echols, N., Headd, J. J., Moriarty, N. W., Mustyakimov, M., Terwilliger, T. C., Urzhumtsev, A., Zwart, P. H., & Adams, P. D. (2012). Towards automated crystallographic structure refinement with phenix.refine. *Acta Crystallographica. Section D, Biological Crystallography*, *68*(Pt 4), 352–367. https://doi.org/10.1107/S0907444912001308

Biancucci, M., Dolores, J. S., Wong, J., Grimshaw, S., Anderson, W. F., Satchell, K. J. F., & Kwon, K. (2017). New ligation independent cloning vectors for expression of recombinant proteins with a self-cleaving CPD/6xHis-tag. *BMC Biotechnology*, *17*(1), 1. https://doi.org/10.1186/s12896-016-0323-4

Blow, D. (2002). *Outline of crystallography for Biologists*. Oxford University press.

Boulanger, M. J., Kukimoto, M., Nishiyama, M., Horinouchi, S., & Murphy, M. E. P. (2000). Catalytic Roles for Two Water Bridged Residues (Asp-98 and His-255) in the Active Site of Copper-containing Nitrite Reductase*. *Journal of Biological Chemistry*, *275*(31), 23957–23964. https://doi.org/10.1074/jbc.M001859200

Boulanger, M. J., & Murphy, M. E. P. (2003). Directing the mode of nitrite binding to a copper-containing nitrite reductase from Alcaligenes faecalis S-6: Characterization of an active site isoleucine. *Protein Science: A Publication of the Protein Society*, *12*(2), 248–256. https://doi.org/10.1110/ps.0224503

Brünger, A. T. (1992). Free R value: A novel statistical quantity for assessing the accuracy of crystal structures. *Nature*, *355*(6359), 472–475. https://doi.org/10.1038/355472a0

Cheng, R., Wu, C., Cao, Z., & Wang, B. (2020). QM/MM MD simulations reveal an asynchronous PCET mechanism for nitrite reduction by copper nitrite reductase. *Physical Chemistry Chemical Physics*, *22*(36), 20922–20928. https://doi.org/10.1039/D0CP03053H

Costentin, C., Robert, M., & Savéant, J.-M. (2013). Catalysis of the electrochemical reduction of carbon dioxide. *Chem. Soc. Rev.*, *42*(6), 2423–2436. https://doi.org/10.1039/C2CS35360A

Cristaldi, J. C., Gómez, M. C., González, P. J., Ferroni, F. M., Dalosto, S. D., Rizzi, A. C., Rivas, M. G., & Brondino, C. D. (2018). Study of the Cys-His bridge electron transfer pathway in a copper-containing nitrite reductase by site-directed mutagenesis,

47

spectroscopic, and computational methods. *Biochimica et Biophysica Acta. General Subjects*, *1862*(3), 752–760. https://doi.org/10.1016/j.bbagen.2017.10.011

Ellis, M. J., Dodd, F. E., Sawers, G., Eady, R. R., & Hasnain, S. S. (2003). Atomic Resolution Structures of Native Copper Nitrite Reductase from Alcaligenes xylosoxidans and the Active Site Mutant Asp92Glu. *Journal of Molecular Biology*, *328*(2), 429–438. https://doi.org/10.1016/S0022-2836(03)00308-5

Emsley, P., Lohkamp, B., Scott, W. G., & Cowtan, K. (2010). Features and development of Coot. *Acta Crystallographica. Section D, Biological Crystallography*, *66*(Pt 4), 486–501. https://doi.org/10.1107/S0907444910007493

Eyal, E., Chennubhotla, C., Yang, L.-W., & Bahar, I. (2007). Anisotropic fluctuations of amino acids in protein structures: Insights from X-ray crystallography and elastic network models. *Bioinformatics*, *23*(13), i175–i184. https://doi.org/10.1093/bioinformatics/btm186

Fujita, E., Muckerman, J. T., & Himeda, Y. (2013). Interconversion of CO2 and formic acid by bio-inspired Ir complexes with pendent bases. *Biochimica et Biophysica Acta (BBA) - Bioenergetics*, *1827*(8), 1031–1038. https://doi.org/10.1016/j.bbabio.2012.11.004

Hosseinzadeh, P., Marshall, N. M., Chacón, K. N., Yu, Y., Nilges, M. J., New, S. Y., Tashkov, S. A., Blackburn, N. J., & Lu, Y. (2016). Design of a single protein that spans the entire 2-V range of physiological redox potentials. *Proceedings of the National Academy of Sciences*, *113*(2), 262–267. https://doi.org/10.1073/pnas.1515897112

Kataoka, K., Furusawa, H., Takagi, K., Yamaguchi, K., & Suzuki, S. (2000). Functional analysis of conserved aspartate and histidine residues located around the type 2 copper site of copper-containing nitrite reductase. *Journal of Biochemistry*, *127*(2), 345–350. https://doi.org/10.1093/oxfordjournals.jbchem.a022613

Leo, F., Schwarz, F. M., Schuchmann, K., & Müller, V. (2021). Capture of carbon dioxide and hydrogen by engineered Escherichia coli: Hydrogen-dependent CO2 reduction to formate. *Applied Microbiology and Biotechnology*, *105*(14–15), 5861–5872. https://doi.org/10.1007/s00253-021-11463-z

Leung, C.-F., & Ho, P.-Y. (2019). Molecular Catalysis for Utilizing CO2 in Fuel Electro-Generation and in Chemical Feedstock. *Catalysts*, *9*(9), Article 9. https://doi.org/10.3390/catal9090760

Li, Y., Hodak, M., & Bernholc, J. (2015). Enzymatic Mechanism of Copper-Containing Nitrite Reductase. *Biochemistry*, *54*(5), 1233–1242. https://doi.org/10.1021/bi5007767

Liebschner, D., Afonine, P. V., Baker, M. L., Bunkóczi, G., Chen, V. B., Croll, T. I., Hintze, B., Hung, L. W., Jain, S., McCoy, A. J., Moriarty, N. W., Oeffner, R. D., Poon, B. K., Prisant, M. G., Read, R. J., Richardson, J. S., Richardson, D. C., Sammito, M. D., Sobolev, O. V., … Adams, P. D. (2019). Macromolecular structure determination using X-rays, neutrons and electrons: Recent developments in Phenix. *Acta Crystallographica. Section D, Structural Biology*, *75*(Pt 10), 861–877. https://doi.org/10.1107/S2059798319011471

McCarthy, A. A., Barrett, R., Beteva, A., Caserotto, H., Dobias, F., Felisaz, F., Giraud, T., Guijarro, M., Janocha, R., Khadrouche, A., Lentini, M., Leonard, G. A., Lopez Marrero, M., Malbet-Monaco, S., McSweeney, S., Nurizzo, D., Papp, G., Rossi, C., Sinoir, J., … Mueller-Dieckmann, C. (2018). ID30B – a versatile beamline for macromolecular crystallography experiments at the ESRF. *Journal of Synchrotron Radiation*, *25*(4), Article 4. https://doi.org/10.1107/S1600577518007166

McPherson, A. (1989). Macromolecular Crystals. *Scientific American*, *260*(3), 62–69.

McPherson, A., & Gavira, J. A. (2014). Introduction to protein crystallization. *Acta Crystallographica. Section F, Structural Biology Communications*, *70*(Pt 1), 2–20. https://doi.org/10.1107/S2053230X13033141

Mueller-Dieckmann, C., Bowler, M. W., Carpentier, P., Flot, D., McCarthy, A. A., Nanao, M. H., Nurizzo, D., Pernot, P., Popov, A., Round, A., Royant, A., Sanctis, D. de, Stetten, D. von, & Leonard, G. A. (2015). The status of the macromolecular crystallography beamlines at the European Synchrotron Radiation Facility. *The European Physical Journal Plus*, *130*(4), Article 4. https://doi.org/10.1140/epjp/i2015-15070-0

Murphy, M. E. P., Turley, S., & Adman, E. T. (1997). Structure of Nitrite Bound to Copper-containing Nitrite Reductase from Alcaligenes faecalis: MECHANISTIC IMPLICATIONS*. *Journal of Biological Chemistry*, *272*(45), 28455–28460. https://doi.org/10.1074/jbc.272.45.28455

Powell, H. R. (2017). X-ray data processing. *Bioscience Reports*, *37*(5), BSR20170227. https://doi.org/10.1042/BSR20170227

Rose, S. L., Antonyuk, S. V., Sasaki, D., Yamashita, K., Hirata, K., Ueno, G., Ago, H., Eady, R. R., Tosha, T., Yamamoto, M., & Hasnain, S. S. (2021). An unprecedented insight into the catalytic mechanism of copper nitrite reductase from atomic-resolution and damage-free structures. *Science Advances*, *7*(1), eabd8523. https://doi.org/10.1126/sciadv.abd8523

REFERENCE LIST

Schrödinger, LLC. (2015). *The PyMOL Molecular Graphics System, Version 2.5.2*.

Schwarz, F. M., Schuchmann, K., & Müller, V. (2018). Hydrogenation of CO2 at ambient pressure catalyzed by a highly active thermostable biocatalyst. *Biotechnology for Biofuels*, *11*(1), 237. https://doi.org/10.1186/s13068-018-1236-3

Taylor, G. L. (2010). Introduction to phasing. *Acta Crystallographica. Section D, Biological Crystallography*, *66*(Pt 4), 325–338. https://doi.org/10.1107/S0907444910006694

Tocheva, E. I., Eltis, L. D., & Murphy, M. E. P. (2008). Conserved Active Site Residues Limit Inhibition of a Copper-Containing Nitrite Reductase by Small Molecules. *Biochemistry*, *47*(15), 4452–4460. https://doi.org/10.1021/bi7020537

Williams, C. J., Headd, J. J., Moriarty, N. W., Prisant, M. G., Videau, L. L., Deis, L. N., Verma, V., Keedy, D. A., Hintze, B. J., Chen, V. B., Jain, S., Lewis, S. M., Arendall, W. B., Snoeyink, J., Adams, P. D., Lovell, S. C., Richardson, J. S., & Richardson, D. C. (2018). MolProbity: More and better reference data for improved all-atom structure validation. *Protein Science: A Publication of the Protein Society*, *27*(1), 293–315. https://doi.org/10.1002/pro.3330

Windle, C. D., & Perutz, R. N. (2012). Advances in molecular photocatalytic and electrocatalytic CO2 reduction. *Coordination Chemistry Reviews*, *256*(21), 2562–2570. https://doi.org/10.1016/j.ccr.2012.03.010

Wlodawer, A., Minor, W., Dauter, Z., & Jaskolski, M. (2013). Protein crystallography for aspiring crystallographers or how to avoid pitfalls and traps in macromolecular structure determination. *The FEBS Journal*, *280*(22), 5705–5736. https://doi.org/10.1111/febs.12495

Yang, J. Y., Kerr, T. A., Wang, X. S., & Barlow, J. M. (2020). Reducing CO2 to HCO2– at Mild Potentials: Lessons from Formate Dehydrogenase. *Journal of the American Chemical Society*, *142*(46), 19438–19445. https://doi.org/10.1021/jacs.0c07965

6 APPENDIX

Method-related; buffers, solvents, etc.

Agar plates with amp

0.5 L LB-agar was made by adding 5g tryptone, 2.5g yeast extract, 5g NaCl and 6g agar with Milli-Q water and storing it at 65 ℃. 500 µL ampicillin (100mg/mL) was added and the mix was poured into Petri dishes in a sterile bench. These were stored in a fridge until used.

Ampicillin 100 mg/mL stock

1g ampicillin in 10 mL Milli-Q. Filtered and stored at -20 ℃ in Eppendorf tubes.

Antifoam

25 % antifoam and 75 % Ethanol

Binding buffer

20mM MOPS, 20 mM imidazole, and 500 mM NaCl. Adjusted to pH 7.4 and filter sterilized.

Cleavage buffer

20mM MOPS, 20mM imidazole, 500 mM NaCl, and 1mM phytic acid. Adjusted to pH 7.4 and filter sterilized.

Elution buffer

20mM MOPS, 500 mM imidazole, and 500 mM NaCl. Adjusted to pH 7.4 and filter sterilized.

IPTG

0.5M IPTG stock made by adding 1.19 g IPTG in 10 mL
Milli-Q water.

LB media

Milli-Q water was added to 5 g of tryptone, 2.5 g of yeast extract and 5 g of NaCl, to a total volume of 0.5 L. The flask was then autoclaved.

NirK SEC buffer

20 mM Tris-HCl and 150 mM NaCl. Adjusted to pH 7 and filter sterilized.

Phosphate buffer

To make 1L, 23g KH_2PO_4 (Potassium dihydrogen phosphate) and 125g K_2HPO_4 (Dibasic potassium phosphate) was measured. Milli-q was added, and pH adjusted to 7. More Milli-Q water was added to a total volume of 1L. this was then filter sterilized.

Soc media (Super Optimal Catabolite)

20 g Bacto tryptone, 5 g yeast extract, 0.58 g NaCl, and 0.186 g KCl was added to a 2 L flask. Milli-Q water was added to the total volume of 1 L and the flask was mixed and autoclaved. 10 mL of a 2M magnesium solution containing 1M magnesium sulfate and 1M magnesium chloride was added as well as 10 mL of 2M glucose, and it was mixed well.

TB media

Milli-Q water was added to 12 g of yeast extract, 6 g of tryptone, and 4 mL of 50% glycerol, to a total wolume of 0.4 L. This was then autoclaved. 100 mL of phosphate buffer with pH 7 was added after the flask was autoclaved, making the total volume 0.5 L.

Storage buffer, Tris HCl pH 7

20mM Tris. Adjusted to pH 7 with HCl and filter sterilized.

SDS page from mutation expression test.

The expression test was performed to make sure that the chosen colonies would grow and express the mutated NiR protein. One parallel of each of the variants was not induced to see the effect the induction had. As the protein must be soluble to be able to purify and crystallize, both the non-soluble and soluble parts were investigated.
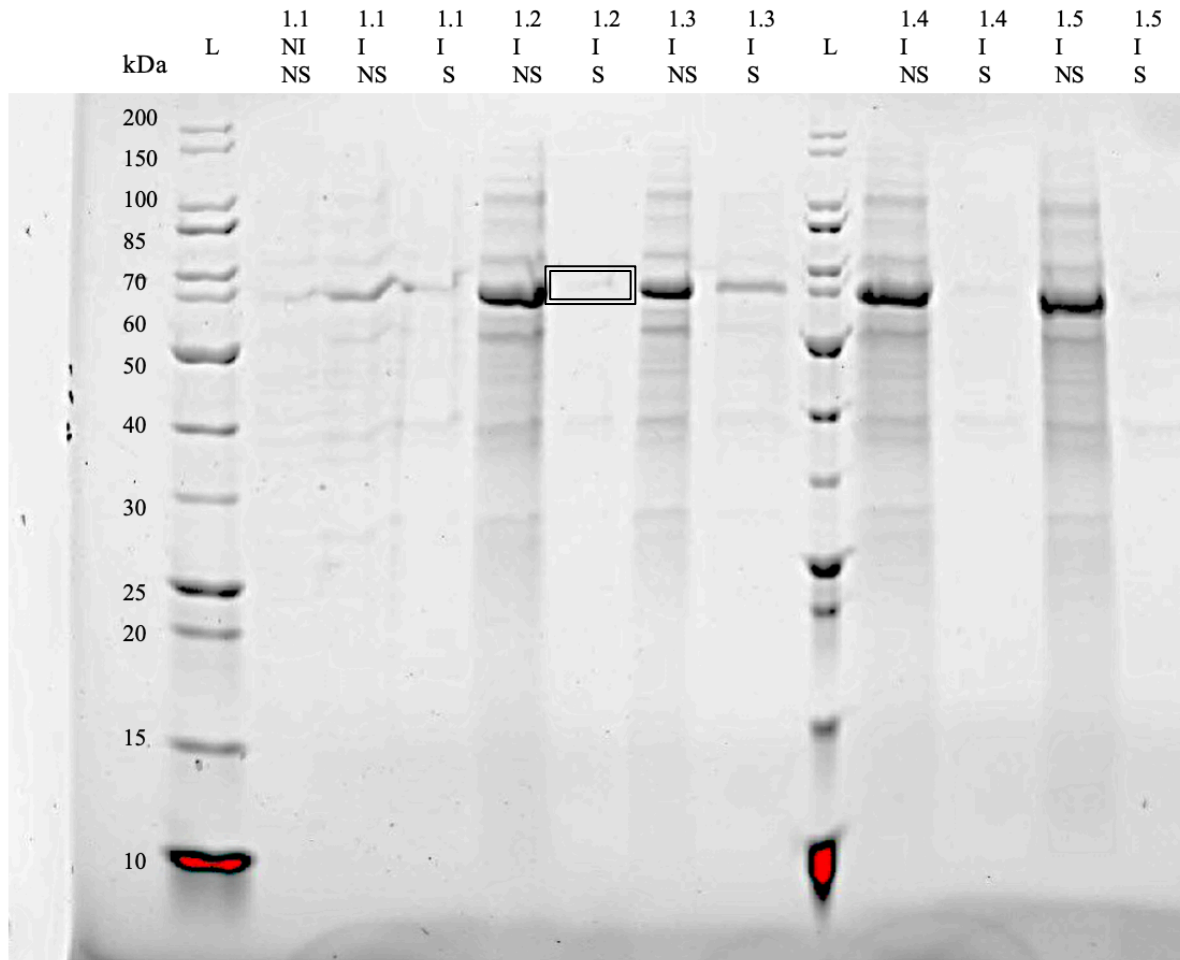

Figure 6.1. SDS-Page of mutation 1, NiR D98E. L = ladder, NI = Not Induced, I = Induced, NS = Non-Soluble, and S = Soluble. The fragments are visible at around 60 kDa because they consist of Cu-NiR with the CPD-tag. There is more protein in the non-soluble fractions than the soluble ones.
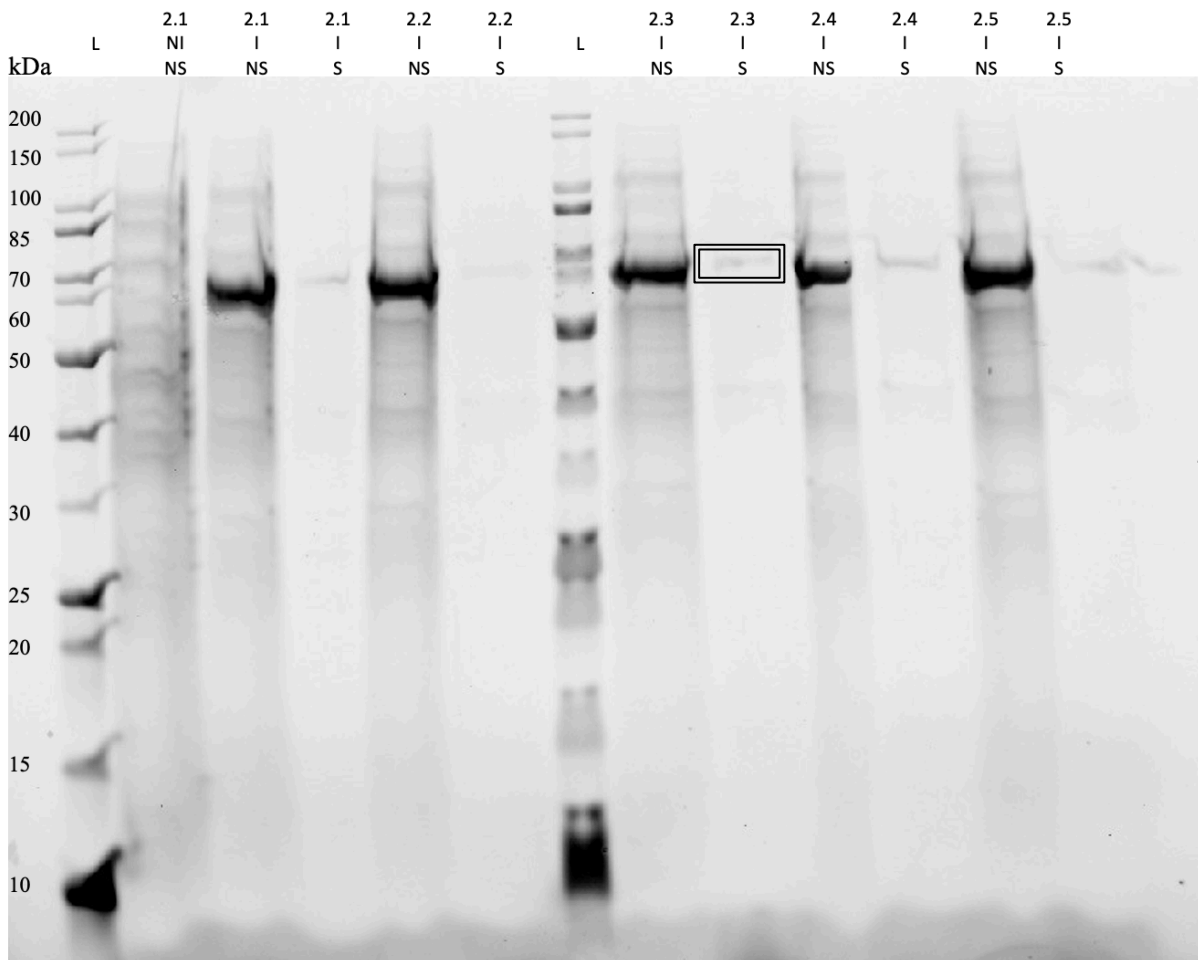
Figure 6.2. *SDS-Page of mutation 2, Nir D98H. L = ladder, NI = Not Induced, I = Induced, NS = Non-Soluble, and S = Soluble. The non-soluble fractions are more visible in this gel compared to D98E in Figure 6.1. The soluble fractions are also slightly less visible. The fragments are about 60 kDa in size, as they are Cu-NiR protein with CPD-tag attached.*

NiR alone is 37.03 kDa, and with the CPD-tag of 23.2 kDa, the fragments end up at 60.23 kDa as seen in the SDS-Page gel. There is less fragments protein in the soluble fractions, but they are still visible. Colony 1.2 was chosen to express the Cu-NiR D98E protein. Colony 2.3 was chosen to express Cu-NiR D98H. This is visualized by the black rectangles.

SDS-Page after SEC purification.
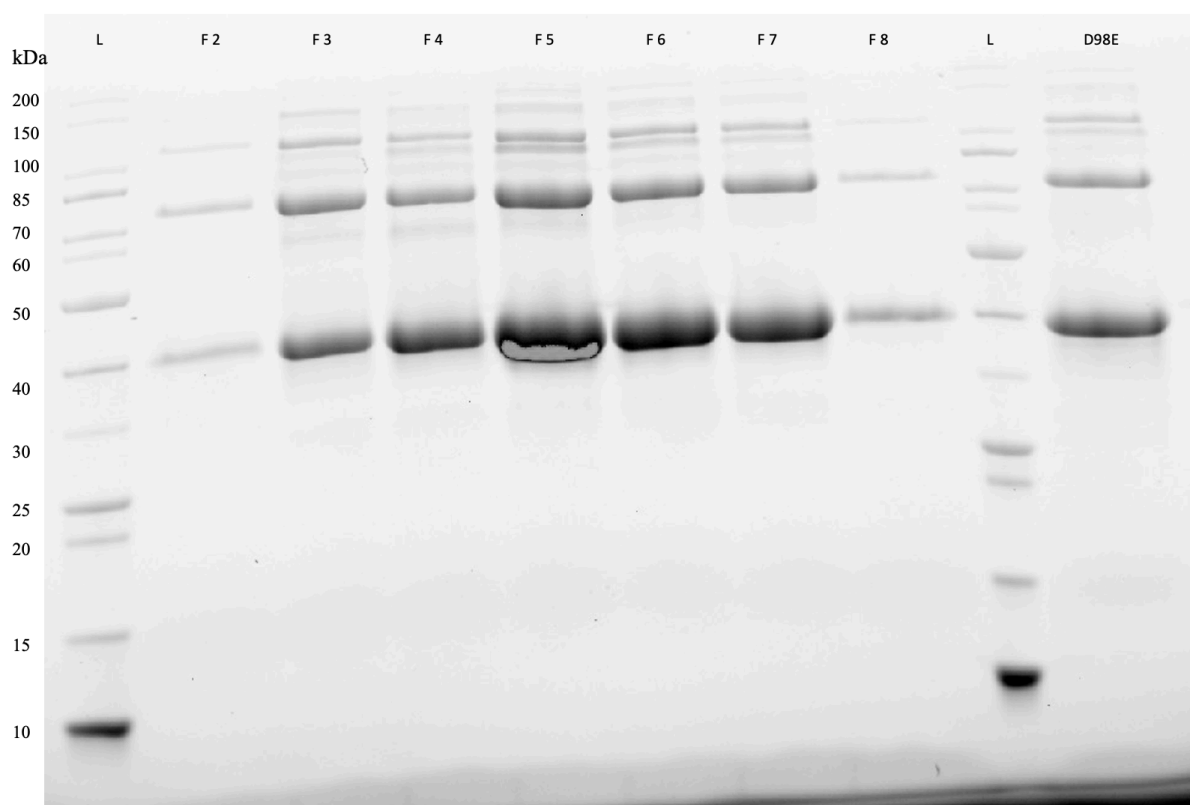
Figure 6.3. *SDS-Page after SEC purification. F2-F8 are the fractions of NiR D98H protein, and the last well contains all fractions of NiR D98E gathered from the SEC purification. F5 shows the strongest signal, matching the peak where most protein was eluted during the purification. The fragments at around 40 kDa are the pure NiR protein which is 37.03 kDa.*

The fragments show the desired NiR proteins at 37.03 kDa, although this batch of purified protein proved difficult to crystallize due to contamination in the SEC column.

Tables of Data collection and refinements statistics of the AfNiR crystals.

*Table 6.1. Crystal data, data collection, and refinements statistics of WT Cu-NiR from X-ray diffraction. *Outer shell values in parenthesis. # crystal from puck 002 position 5, soaked in solution 2A. ## crystal from puck 006 position 5, soaked in solution 2B.*

WT	ox Cu-NiR, no formate	ox Cu-NiR, formate	red Cu-NiR, no formate #	red Cu-NiR, no formate ##	red Cu-NiR, formate
Crystal data					
Space group	$P2_12_12_1$	$P2_12_12_1$	$P2_12_12_1$	$P2_12_12_1$	$P2_12_12_1$
Crystal parameters	a=61.019Å, b=102.203Å, c=146.280Å	a=61.03Å, b=102.57Å, c=145.97Å	a= 61.2740Å, b=102.5760Å, c=146.3980Å	a=61.60Å, b=102.63Å, c=146.62Å	a=61.55Å, b=102.44Å, c=146.01Å
	α = 90.0°, β = 90.0°, γ = 90.0°	α = 90.0°, β = 90.0°, γ = 90.0°	α = 90.0°, β = 90.0°, γ = 90.0°	α = 90.0°, β = 90.0°, γ = 90.0°	α = 90.0°, β = 90.0°, γ = 90.0°
Data collection					
X-ray source	ESRF, ID30B	ESRF, ID30B	ESRF, ID30B	ESRF, ID30B	ESRF, ID30B
Resolution (Å)*	83.78-1.436 (1.461-1.436)	48.66-1.32 (1.37-1.32)	48.80-1.44 (1.49-1.44)	73.31-1.54 (1.57-1.54)	73.01-1.32 (1.34-1.32)
Wavelength (Å)	0.87313	0.87313	0.87313	0.87313	0.87313
Temperature (K)	100 K	100 K	100 K	100 K	100 K
Number of unique reflections*	166990 (8271)	213951 (20410)	167103 (16266)	136451 (6156)	216712 (9878)
Completeness *	100.0 (99.8)	99.6 (97.8)	100.0 (100.0)	98.9 (91.8)	99.5 (92.3)
Redundancy*	7.4 (5.5)	7.4 (6.4)	7.5 (7.8)	5.0 (5.2)	6.9 (3.7)
CC half*	0.997 (0.396)	0.999 (0.579)	0.999 (0.423)	0.998 (0.578)	0.999 (0.566)
Mean(I)/sd(I)*	7.2 (0.7)	13.5 (1.1)	13.2 (0.8)	11.0 (1.2)	13.2 (1.0)
R_{merge} (all I+ & I-) *	0.107 (1.953)	0.065 (1.352)	0.062 (2.382)	0.066 (0.985)	0.069 (0.955)
Refinement statistics					
R_{work}	0.1634	0.1597	0.1704	0.1573	0.1595
R_{free}	0.1921	0.1853	0.1959	0.1882	0.1824
Wilson B-factor (Å²)	20.02	16.38	22.94	22.93	15.23
Ramachandran plot, in most favoures/ other allowed regions (%)	99.1/0.9	99.3/0.7	99.2/0.8	98.91/1.09	99.2/0.8

Table 6.2. *Crystal data, data collection, and refinements statistics of D98E Cu-NiR from X-ray diffraction. *Outer shell values in parenthesis.*

D98E	Ox Cu-NiR, no formate	ox Cu-NiR, formate	red Cu-NiR, no formate	red Cu-NiR, formate
Crystal data				
Space group	$P2_12_12_1$	$P2_12_12_1$	$P2_12_12_1$	$P2_12_12_1$
Crystal parameters	a=60.9030 Å, b=102.0740 Å, c=145.8450 Å	a=60.9370 Å, b=102.2890 Å, c=145.4740 Å	a=61.596 Å, b=102.700 Å, c=146.208 Å	a=102.9100 Å, b=146.2740 Å, c=61.4130 Å
	α = 90.0˚, β = 90.0˚, γ = 90.0˚	α = 90.0˚, β = 90.0˚, γ = 90.0˚	α = 90.0˚, β = 90.0˚, γ = 90.0˚	α = 90.0˚, β = 90.0˚, γ = 90.0˚
Data collection				
X-ray source	ESRF, ID30B	ESRF, ID30B	ESRF, ID30B	ESRF, ID30B
Resolution (Å)*	49.23-1.76 (1.82-1.76)	49.26-1.72 (1.78-1.72)	73.104-1.331 (1.421-1.331)	48.76-1.39 (1.44-1.39)
Wavelength (Å)	0.87313	0.87313	0.87313	0.87313
Temperature (K)	100 K	100 K	100 K	100 K
Number of unique reflections*	90614 (8653)	97263 (9427)	173828 (8691)	186223 (18064)
Completeness*	99.7 (98.2)	99.9 (99.9)	spherical: 81.9 (23.3), ellipsoidal: 95.7 (63.1)	99.9 (100.0)
Redundancy*	6.1 (5.5)	7.1 (6.1)	5.5 (2.9)	5.6 (5.8)
CC half*	0.996 (0.548)	0.997 (0.585)	0.995 (0.663)	0.999 (0.576)
Mean(I)/sd(I)*	6.7 (0.8)	9.8 (1.2)	8.8 (1.5)	9.8 (1.0)
R_{merge} (all I+ & I-) *	0.132 (1.320)	0.118 (1.265)	0.088 (0.564)	0.088 (1.491)
Refinement statistics				
R_{work}	0.1682	0.1560	0.1682	0.1675
R_{free}	0.2046	0.1953	0.1882	0.1910
Wilson B-factor (Å^2)	27.82	24.56	14.25	16.37
Ramachandran plot, in most favoures/ other allowed regions (%)	98.71/1.29	99.11/0.89	99.4/0.6	99.3/0.7

*Table 6.3. Crystal data, data collection, and refinements statistics of D98H Cu-NiR from X-ray diffraction. *Outer shell values in parenthesis.*

D98H	ox Cu-NiR, no formate	ox Cu-NiR, formate	red Cu-NiR, no formate	red Cu-NiR, formate
Crystal data				
Space group	$P2_12_12_1$	$P2_12_12_1$	$P2_12_12_1$	$P2_12_12_1$
Crystal parameters	a= 61.3310 Å, b= 102.5630 Å, c= 146.2750 Å	a= 61.08 Å, b= 102.10 Å, c= 146.14 Å	a= 61.7000 Å, b= 102.8610 Å, c= 146.0500 Å	a= 60.9300 Å, b= 102.2500 Å, c= 146.2930 Å
	α = 90.0°, β = 90.0°, γ = 90.0°	α = 90.0°, β = 90.0°, γ = 90.0°	α = 90.0°, β = 90.0°, γ = 90.0°	α = 90.0°, β = 90.0°, γ = 90.0°
Data collection				
X-ray source	ESRF, ID30B	ESRF, ID30B	ESRF, ID30B	ESRF, ID30B
Resolution (Å)*	48.76-1.71 (1.77-1.71)	73.07-1.64 (1.67-1.64)	48.68-1.43 (1.48-1.43)	48.761.44 (1.49-1.44)
Wavelength (Å)	0.87313	0.87313	0.87313	0.87313
Temperature (K)	100 K	100 K	100 K	100 K
Number of unique reflections*	98942 (8841)	112636 (5444)	171769 (16668)	165546 (16119)
Completeness*	99.1 (91.5)	99.8 (98.7)	100.0 (99.9)	100.0 (100.0)
Redundancy*	6.9 (4.4)	7.3 (5.7)	7.0 (5.5)	7.5 (7.8)
CC half*	0.994 (0.538)	0.998 (0.582)	0.998 (0.573)	0.999 (0.701)
Mean(I)/sd(I)*	7.3 (0.9)	11.1 (1.1)	10.2 (1.2)	15.2 (1.5)
R_{merge} (all I+ & I-) *	0.139 (1.021)	0.090 (1.371)	0.128 (1.309)	0.060 (1.240)
Refinement statistics				
R_{work}	0.1740	0.1699	0.1587	0.1798
R_{free}	0.2057	0.2070	0.1795	0.2011
Wilson B-factor ($Å^2$)	25.65	24.86	14.81	18.66
Ramachandran plot, in most favoures/ other allowed regions (%)	98.9/1.1	99.1/0.9	99.5/0.5	99.3/0.7